Geochimica et Cosmochimica Acta
February 2017, Volume 199 Pages 222-237
http://dx.doi.org/10.1016/j.gca.2016.11.037
http://archimer.ifremer.fr/doc/00363/47399/

The open sea as the main source of methylmercury in the water column of the Gulf of Lions (Northwestern Mediterranean margin)

Cossa Daniel [1, 2, *], Durrieu De Madron Xavier [3], Schäfer Jörg [4], Lanceleur Laurent [4], Guédron Stéphane [2], Buscail Roselyne [3], Thomas Bastien [5], Castelle Sabine [1], Naudin Jean-Jacques [6]

[1] Ifremer, Mediterranean Centre, BP 330, F-83507 La Seyne-sur-Mer, France
[2] Université Grenoble Alpes, ISTerre, BP 53, F-38041 Grenoble, France
[3] Université de Perpignan, Cnrs-Cefrem, 52, Ave. P. Alduy, F-66860 Perpignan Cedex, France
[4] Université de Bordeaux, Epoc, F-33615 Pessac, France
[5] Ifremer, Atlantic Centre, BP 21105, F-44311 Nantes Cedex 03, France
[6] Université P. et M. Curie, Lobb, F-66651 Banyuls-sur-Mer, France

* Corresponding author : Daniel Cossa, email address : dcossa@ifremer.fr

Abstract :

Despite the ecologic and economical importance of coastal areas, the neurotoxic bioaccumulable monomethylmercury (MMHg) fluxes within the ocean margins and exchanges with the open sea remain unassessed. The aim of this paper is to address the questions of the abundance, distribution, production and exchanges of methylated mercury species (MeHgT), including MMHg and dimethylmercury (DMHg), in the waters, atmosphere and sediments of the Northwestern Mediterranean margin including the Rhône River delta, the continental shelf and its slope (Gulf of Lions) and the adjacent open sea (North Gyre).

Concentrations of MeHgT ranged from <0.02 to 0.48 pmol L−1 with highest values associated with the oxygen-deficient zone of the open sea. The methylated mercury to total mercury proportion (MeHgT/HgT) increased from 2% to 4% in the Rhône River to up to 30% (averaging 18%) in the North Gyre waters, whereas, within the shelf waters, MeHgT/HgT proportions were the lowest (1–3%). We calculate that the open sea is the major source of MeHgT for the shelf waters, with an annual flux estimated at 0.68 ± 0.12 kmol a−1 (i.e., equivalent to 12% of the HgT flux). This MeHgT influx is more than 80 times the direct atmospheric deposition or the in situ net production, more than 40 times the estimated “maximum potential” annual efflux from shelf sediment, and more than 7 times that of the continental sources. In the open sea, ratios of MMHg/DMHg in waters were always <1 and minimum in the oxygen deficient zones of the water column, where MeHg concentrations are maximum. This observation supports the idea that MMHg could be a degradation product of DMHg produced from inorganic divalent Hg.

Keywords : Mercury, Methylmercury, Ocean margin, Coastal area, Mediterranean

1. Introduction

Mercury (Hg) exists in the marine environment as elemental Hg (Hg^0) and divalent Hg species, which include various inorganic (Hg^{II}_i) species (e.g., chlorocomplexes) and the two methylated species: monomethylmercury (MMHg) and dimethylmercury (DMHg). Monomethylmercury is a neurotoxin that bioaccumulates in aquatic organisms and biomagnifies through trophic webs (e.g., Jensen and Jernelov, 1969; Clarkson and Magos, 2006). However, despite the ecological and economical importance of coastal areas, especially in terms of fish and shellfish production and capture, the distributions, sources and fluxes of methylated Hg species in the waters of the ocean margins are still poorly explored.

Methylated Hg sources for coastal waters include (i) inputs from upwellings, rivers, groundwaters, atmospheric deposition and waste water point sources, and (ii) *in situ* Hg^{II}_i methylation in coastal waters and sediments (Cossa et al., 1996; Fitzgerald et al., 2007). The river-watershed contribution can be large due to direct inputs of MMHg to coastal waters (Coquery et al., 1997; Choe and Gill, 2003; Balcom et al., 2008 and 2015; Muresan et al., 2008; Guédron et al., 2012; Buck et al., 2015) and continental groundwaters *via* submarine estuaries (Ganguli et al., 2012). Contribution of the open ocean to the methylated Hg load of oceanic margin waters has also been evidenced: DMHg is conveyed, *via* upwellings, from ocean interior to surface coastal waters (Conaway et al., 2009). Atmosphere has been reported

as external methylated Hg sources, but available data are limited (e.g., Weiss-Penzias et al., 2012 and 2016). In situ Hg methylation has been observed in both coastal sediments (e.g., Gobeil and Cossa, 1993; Hammerschmidt et al., 2004; Hammerschmidt and Fitzgerald, 2006; Balcom et al., 2008; Hollweg et al., 2009 and 2010; Luengen and Flegal, 2009; Noh et al., 2013) and waters (Mason et al., 1993; Sunderland et al., 2010; Lehnherr et al., 2011; Wang et al., 2012; Lehnherr, 2014; Schartup et al., 2015). Experimental MMHg production from incubation of settling particles ("marine snow") or water strongly suggests that water column methylation may be important worldwide (Monperrus et al., 2007; Ortiz et al., 2015). In summary, numerous internal and external sources of methylated Hg in coastal waters exist; however, their relative importance is not well established.

Pathways of Hg methylation in both oceanic and coastal waters are still poorly described, despite the oceanographically-consistent measurements of methylated Hg performed for three decades in the waters of the Atlantic Ocean (Mason et al., 1998; Mason and Sullivan, 1999; Bowman et al., 2015), the Pacific Ocean (Mason and Fitzgerald, 1990; Hammerschmidt and Bowman, 2012; Munson et al., 2015), and the Mediterranean Sea (Cossa et al., 1994, 1997 and 2009; Horvat et al., 2003). The highest concentrations of methylated Hg are consistenly found in the oxygen deficient zones (ODZs). The generally significant correlation between methylated Hg and oxygen consumption (or organic carbon regeneration rates) have been interpreted as the result of net microbiological Hg^{II}_i methylation at these depths (e.g., Mason and Fitzgerald, 1990; Cossa et al., 2009; Sunderland et al., 2009). The MMHg/DMHg molar ratios in the ODZs vary broadly (0.2 to >10) depending on location, even in the same oceanic region. Early North Atlantic data suggests that MMHg is a degradation product of DMHg in the water column (Fitzgerald and Mason, 1996; Mason et

al., 1998; Mason and Sullivan, 1999). However, production rate measurements, performed on Arctic waters, found contradictory results (Lehnheer et al., 2011). These authors found that DMHg production from Hg^{II}_i was two orders of magnitude less than MMHg production, but faster than the rate of DMHg production from MMHg methylation. Consistent with these findings, recent results show that MMHg is the dominant form of methylated Hg in deep waters of the North Atlantic (Bowman et al., 2015). More recently, Jonsson et al. (2016) suggest that MMHg can be methylated on sulfide mineral surfaces, a pathway potentially responsible for much of the DMHg in oceanic waters. In summary, data on MMHg and DMHg distributions in marine waters are still scarce (especially in coastal areas), and, consequently, the methylation mechanism of Hg^{II}_i remains uncertain.

In the present work, we address questions of abundance, distribution, production and exchanges of methylated Hg in the waters of the Northwestern Mediterranean margin including the Rhône River delta, the continental shelf and its slope (Gulf of Lions), the continental rise and the adjacent open sea (North Gyre) (Fig. 1). The objective is to assess the relative importance of internal and external sources of methylated Hg in the context of marine Hg cycle. For this, we have (i) monitored atmospheric deposition and riverine inputs of total methylated Hg (MeHgT = MMHg + DMHg), (ii) studied the MeHg distribution within the Rhône River plume, the freshwater–sea water mixing zone, the continental shelf-slope-rise system, and the adjacent open sea, and (iii) estimated the MeHg exchanges across various interfaces, including water/sediment and coastal/off-shore water interface. Additional data of total Hg (HgT = all the Hg species) were also collected in order to estimate the importance of MeHg fraction.

2. Study area

The Northwestern Mediterranean is characterized by the presence of a large continental shelf and the associated slope, both constituting the Gulf of Lions (Fig. 1). The water circulation in the Gulf of Lions is influenced in the South by the Northern Current, which is a part of a current system going from the Tyrrhenian Sea up to the Alboran Sea (Millot and Tapier-Letage, 2005). This Northern Current flows as a major vein along the upper part of the continental slope intruding onto the shelf (Fig. 1). The North Gyre and Gulf of Lions have contrasting hydrological and biological properties. The North Gyre is a typical oligotrophic open Mediterranean environment experiencing strong winter mixing of the surface and intermediate water masses, whereas the Gulf of Lions constitutes one of the few mesotrophic coastal regions within the Mediterranean Sea (Morel and André, 1991) largely influenced by the Rhône River freshwater inputs.

The Gulf of Lions receives riverine inputs mainly from the Rhône River. The Rhône River is the major freshwater input to the western Mediterranean and its waters undergo three main processes before being diluted in the Gulf of Lions waters. First, freshwater is rapidly mixed with seawater within the few kilometers between Barcarin and the prodelta area (Fig. 1) (Elbaz-Poulichet et al., 1996). Secondly, the Rhône River plume is driven on the shelf by changeable continental winds (the northerly Mistral, southwesterly Tramontane and southeasterly-easterly Marin) and the cyclonic Northern Current (Fig. S1) (Naudin et al., 1997). The plume is periodically broken due to wind direction changes, producing “Low Salinity Water” lenses drifting on the shelf Naudin et al. (1997). Thirdly, below the Rhône River plume, the dense riverine particles settle abruptly, generating large sediment accumulation in the prodelta area up to several tens of centimeters per year in the proximal

delta (~ 20 m) according to Charmasson et al. (1998), Radakovitch et al. (1999), Maillet et al. (2006) and Cathalot et al. (2010). Finer riverine material is exported farther on the Gulf of Lions shelf, undergoing a westward net transport through sedimentation/resuspension processes generated by infrequent easterly wind storm events (Durrieu de Madron et al., 2008; Ulses et al., 2008; Guizien, 2009; Marion et al., 2010; Bourrin et al., 2015).

3. Material and methods

To summarize the nomenclature used in the following text, X_{UNF}, X_F and X_P refer to unfiltered, dissolved (< 0.45 μm) and particulate, respectively (with X being a Hg species). Detailed protocols of the sampling and analytical techniques are given in SI 1. Sampling and water sample treatments were performed using ultraclean protocols, including acid cleaning of the plastic ware, and the use of plastic gloves and high purity grade reagents (e.g., SUPRAPUR HCl from Merck®, ULTREX HNO_3 from J.T. Baker®).

3.1. Sampling

Sampling cruise identifications, locations and dates are summarized in Table S1.

Atmospheric deposition. Thirteen rain events were collected between April 2009 and January 2010 at a coastal site (La Seyne-sur-Mer, 43°.06.350'N; 5°53.117'E, Fig.1), located at the eastern end of the Gulf of Lions. The unfiltered samples were collected in Teflon (FEP) bottles and acidified (0.4 % v/v HCl) immediately after the water collection. The rain-collecting device (PP040, MTX®) was located 15 m above sea level. Details of the sampling are given by Castelle (2010). At the same site, 28 aerosol samples were collected on cellulose acetate membranes (0.22 μm) from July 2009 to March 2010. Each sample represents one

147 week of pumping at a pumping rate of 14 L min^{-1}. Total gaseous Hg concentrations in the
148 atmosphere were monitored at the same time (Marusczak et al., 2015).

149 *Rhône River monitoring.* Rhône River Hg monitoring was performed over two monitoring
150 periods at Arles (Sta. SORA, Fig. 1): (i) a period of low river waters from March, 2009 to June,
151 2010, with only one rather weak flood event (~3000 m^3 s^{-1} on December the 2nd), and (ii)
152 during the flooding period of October-November 2008 (up to 3580 m^3 s^{-1}). Surface freshwater
153 samples were collected twice a month at Station SORA in Arles (Fig. 1) by pumping through
154 polyethylene tubing using an all-Teflon (PFA) double-bellows pump (10-LPM, ASTI®).
155 Samples were collected in Teflon (FEP) bottles then filtered through hydrophilic Teflon
156 membranes (LCR, Millipore®) with a porosity of 0.45 µm. Membranes were stored at -18°C
157 in polycarbonate Petri dishes and the filtrates were acidified (0.4 % v/v HCl) and stored in
158 Teflon (FEP) bottles.

159 *Rhône delta mixing zone*. Brackish surface waters were sampled on 16 and 17 October 2008
160 from a rubber boat between Barcarin (Rhône River) and the sea (Fig.1); the locations of the
161 stations are indicated on Table S2a. The samples were collected directly into Teflon (FEP)
162 bottles. Samples were then filtered and stored as described in the previous section.

163 *BIOPRHOFI cruise.* During the BIOPROHFI cruise (14th – 27th May 2006), two types of waters
164 were sampled: (i) the productive shelf waters and (ii) the mesotrophic slope waters. In the first
165 type, two Low Salinity Waters, originating from the Rhône River plume, were successively
166 tracked using a Lagrangian sampling protocol: lens "1" between May 14th and 18th,
167 corresponding to stations S1 to S68 and lens "2" between the 19th and 26th, corresponding to
168 stations S88 to S220 (Fig. S2). In the lenses, the 0-50 m layer was sampled by pumping with
169 the all-Teflon pneumatic pump (10-2PM, ASTI®) and through polyethylene tubing, directly

into a class 100 on-board clean laboratory; the water depth varied between 60 and 100 m during the drifting. Two deep casts (0-900 m) were performed on May the 26th at the slope foot (Stas. S221 and S230, Fig. S2); their coordinates are given in Table S2a.

CASCADE cruise. During the CASCADE cruise (1st – 23th March 2011), water was collected (i) on the inner shelf from the Rhône prodelta to the south-western end (Stas. A to D), (ii) at the head of Cap de Creus canyon (Sta. E), and (iii) thirteen deep casts on the shelf edge (Stas. L-01 and M-12), the slope foot (Stas. L-03 and M-10) and within the North Gyre (Stas. Antarès, S2400, L-05-08-10-12 and M-03-05-08) (Fig. 1). Two to twelve water depths were sampled for each cast depending on the height of the water column (Fig. 1 and Table S2). Sediment cores were collected along the Gulf of Lions shelf, at the head of the Cap de Creus canyon and in the abyssal plain in the North Gyre area during the CASCADE cruise (Table S2b). A multicore sampler (Oktopus GmbH Multiple corer with 8 tubes of 100 mm diameter) allowing the sampling of the undisturbed benthic interface (Barnett et al., 1984) was used.

3.2. Sample treatment

Water and particles. The samples from the 0-50 m layer of the shelf waters during the BIOPRHOFI cruise were filtered through polycarbonate membranes (0.45 µm, Nuclepore®). Filtrate was collected in Teflon (FEP) bottles and acidified with HCl (0.4 %, v/v). The collection of particles from the Low Salinity Waters, for subsequent $MMHg_P$, particulate carbon and phosphorus, and pigments determinations, was performed using in-line filtration through pre-heated glass fiber filters (GF/G, Whatman®). Deep-water samples (> 50 m) were collected during the BIOPRHOFI and CASCADE cruises by rosette-mounted 5L bottles (1010X-Niskin, General Oceanics®) equipped with a CTD probe. These samples were not filtered and were analyzed only for HgT_{UNF} and $MeHgT_{UNF}$. Total Hg was determined on board, whereas

MMHg and MeHgT analyses were performed in the laboratory within 2 months after the cruise on the acidified samples stored in the dark at +4°C in a double wrapping of polyethylene bags.

Sediment pore water: The sediment pore water was extracted, from below the sediment surface (-1 cm), using Milli-Q (Millipore®) water-rinsed microporous polymer tube samplers (Rhizon SMS, Rhizosphere Research Products®) attached to an acid washed all-polypropylene syringe (Guédron et al., 2012).

3.3. Chemical analyses

Total mercury. Total Hg, in filtered and unfiltered samples, was measured on board within a few minutes of sampling. The release of Hg from its ligands was achieved by addition of a BrCl solution. This technique is known as the Environmental Protection Agency from the United States of America standard method N° 1631 (www.epa.gov/sites/production/files/2015-08/documents/method_1631e_2002.pdf). The detection limit (DL = 3 times the standard deviation of the blank) was 0.1 pmol L^{-1} and the reproducibility varied according to the concentration level between 5 and 15 % (Cossa et al. 2003). The accuracy of HgT measurements was tested using the ORMS-3 water sample, which is a certified reference material (CRM) from the National Research Council of Canada. Our measurements were always within the confidence limits given for the CRM (12.6 ± 1.1 pg mL^{-1}; http://inms-ienm.nrc-cnrc.gc.ca/calserv/crm_files_f/ORMS-3_f.pdf).

Methylated Hg species. Total methylated Hg and MMHg were measured on filtered and unfiltered samples and DMHg was calculated as the difference between $MeHgT_{UNF}$ and $MMHg_{UNF}$. Since DMHg is converted into MMHg at low pH (Mason, 1991; Black et al., 2009a) MeHgT was determined on acidified samples. Monomethyl Hg was determined after

bubbling samples for 40 min with argon in order to remove DMHg before acidification. Total methylated Hg and MMHg were determined as volatile MMHg hydride by purge and cryo-trapping gas chromatography and detected as elemental Hg vapor by atomic fluorescence spectrometry according to Stoichev et al. (2004). The mercury hydrides (from MMHg and Hg^{II}_i) were formed with $NaBH_4$, sparged from the sample with helium, concentrated and then separated by cryogenic chromatography before detection. During this set of analyses, the low blank (< 0.01 pmol) and its reproducibility (2 %) allowed and limits of quantification (LQ) as low as 0.005 and 0.015 to 0.075 pmol L^{-1}, respectively. The analytical reproducibility varied with time between 6 and 15 %.

$MeHgT_P$ was determined by atomic fluorescence spectrometry after acid extraction, ethylation and chromatographic separation according to Liang et al. (1994). The analytical performances were established by analyzing a Certified Reference Material from the International Atomic Energy Agency (IAEA-142, Horvat et al., 1997). The reproducibility was 10 % and the DL 20 pmol g^{-1}; recovery varied from 80 to 100 %.

Isotopic incubations. Incubation experiments were performed onboard immediately after sampling using a $^{199}Hg^{II}$ stable isotope spike to study Hg methylation potentials in Mediterranean bottom water samples as described for tropical lake water incubations in Huguet et al. (2010). These experiments aimed at simulating the temporal resuspension of reducing sediments in oxic bottom water and evaluating their impact on gross methylation compared to that in bottom water without sediment resuspension. For this, we determined gross methylation in (a) unfiltered bottom water and (b) slurries of surface sediment resuspended in unfiltered bottom water as follows:

238 - (a) Aliquots of unfiltered seawater from the bottom of the shelf water column
239 were transferred into acid-cleaned 125 mL Teflon (FEP) bottles, spiked with $^{199}Hg^{II}$ (Oak
240 Ridge, 92 % purity) to a nominal concentration of 1000 ng $^{199}Hg^{II}$ L^{-1} and incubated at
241 constant temperature (12 °C) in the dark for 48, 96 and 192 hours (n = 2 for each time;
242 manual shaking twice per day). Aliquots (n = 2) of unfiltered bottom water were spiked
243 and methylation was immediately stopped for control. After each incubation time,
244 methylation was stopped by adding 1 mL of 12 M HCl (INSTRA analyzed, J.T. Baker®)
245 and the bottles were stored in double sealed polypropylene bags at 4°C and in the dark
246 until analysis for isotopic composition of the different Hg species.

247 - (b) Surface sediments from the shelf at Stations A to D were added to 100 ml of
248 unfiltered bottom water from the respective site to obtain a nominal suspended particle
249 concentration of 100 mg L^{-1}; three aliquots per site) in acid-cleaned 125 mL Teflon (FEP)
250 bottles, to simulate resuspension events.

251 The slurries were then spiked with $^{199}Hg^{II}$ (Oak Ridge, 92 % purity) to a nominal
252 concentration of 25 ng of Hg per gram of sediment slurry, including water and sediment,
253 and incubated at constant temperature (12 °C) in the dark for 192 hours. Incubation was
254 stopped by freezing (-20°C). The samples were stored frozen, freeze-dried and stored
255 cool in the dark until extraction with HNO_3 (6M, ULTREX, J.T. Baker®) and analysis. The
256 applied protocol including derivation (propylation with $NaBPr_4$), extraction and the
257 analytical setup, i.e. gas chromatography (Focus GC, Thermo Fischer Scientific®)
258 coupled to ICP-MS (X7, Thermo Fischer Scientific®) using a thermostatic interface is
259 based on the methods described in detail elsewhere (Monperrus, 2004). The difference
260 between the $MM^{199}Hg$ measured and the $MM^{199}Hg$ naturally present (calculated from the

amount of $MM^{200}Hg$ measured) represents the $MM^{199}Hg$ produced during the incubation of the $^{199}Hg^{II}$ added. Methylation potential was estimated by dividing the amount of $MM^{199}Hg$ formed by the amount of $^{199}Hg^{II}$ recovered after the respective incubation periods, as described by Monperrus et al. (2007).

Particulate organic carbon, phosphorus and pigments. Particulate organic carbon concentrations were measured according to Hedges and Stem (1984) with a Shimadzu® analyzer (TOC-5000 Series). Soluble reactive phosphorus (SRP) was determined in seawater with an auto-analyzer using the standard molybdate blue method (Murphy and Riley, 1962) as detailed in the protocol by Aminot and Kérouel (2007). Particulate phosphorus (P_P) determination used the same colorimetric method but after magnesium nitrate oxidation (Ormaza-Gonzalez and Statham, 1996). Chlorophyll pigments were determined following the standard method by Strickland and Parsons (1972).

4. RESULTS

4.1. Atmospheric deposition

Total Hg concentrations in unfiltered rain water varied from 10 to 80 pmol L^{-1}, with a mean of 31 ± 22 pmol L^{-1} (n = 13), whereas MeHgT concentrations varied from 0.10 to 1.25 pmol L^{-1}, with a mean of 0.59 ± 0.33 pmol L^{-1} (n = 13), i.e., ~2% of the HgT. These ranges are similar to those published for other coastal areas of the Northern Hemisphere (e.g., Hammerschmidt et al., 2007; Marusczak et al., 2011; Weiss-Penzias et al., 2012). Methylated Hg concentrations in the 28 aerosol samples were undetectable due to the too-small amount of sample collected on the membrane.

4.2. Rhône River and its plume

During the low flow period $MeHg_F$ and $MeHg_P$ concentrations varied in the picomolar range (Table 1), MeHg being predominantly (90%) associated with suspended particles. The mean methylated Hg fractions (MeHg/HgT) were 4 and 2 % as dissolved and particulate, respectively.

The variations of dissolved MeHg concentrations ($MeHgT_F$) during the mixing of Rhône freshwater with Gulf of Lions saltwater, between Barcarin ferry and the prodelta area, are illustrated in Figure 2a. Concentrations of $MeHgT_F$ varied from 0.02 to 0.14 pmol L^{-1} and the distribution follows a conservating mixing line ($R^2 = 0.75$, $p < 0.01$) with higher concentrations in the freshwater and lower concentrations in the seawater end-member (Fig. 2a), similarly to observations of Noh et al. (2013) in the Mekong River delta.

At the bottom of the Low Salinity Waters lenses (~50m), salinity ranged from 38.2 to 38.4, which are typical values for waters of the Northern Current. The lowest salinity in the Low Salinity Waters (32.5) at surface indicates a ~20 % dilution of marine waters with the Rhône River waters. The $MeHgT_F$ concentrations were in the femtomolar range, with 35 % of values lower than the LQ (i.e., <0.015 pmol L^{-1}) and maximum concentration of 0.069 pmol L^{-1} (Table 2). $MeHgT_F$ fraction varies from <0.3 to 5.5 %, averaging 1.5 ± 1.0 % of the HgT_F. The time series of $MeHgT_F$ concentrations in the Low Salinity Waters varied little with depth (Fig. 3). Interesting to note is that high $MeHgT_F$ concentrations occurred at the highest salinities, suggesting a marine MeHg source (Fig. 2b).

4.3. Vertical profiles along shelf and slope

On the shelf, average $MeHgT_{UNF}$ concentrations were 0.026 ± 0.024 pmol L^{-1} (n = 40) (Table 3 and Fig. 4a). The $MeHgT_{UNF}$ / HgT_{UNF} ratios averaged roughly 2 %, ranging from 0.1 to 6.3 % (Table 3).

Tables 2 and 3 summarize the results obtained for the "slope foot" (900-1800m bottom depth) water column in May 2006 (Sta. S-230, BIOPRHOFI cruise) and in March 2011 (Sta. L-03 and M-10, CASCADE cruise). Concentrations of $MeHgT_{UNF}$ ranged from 0.02 to 0.38 pmol L^{-1}, averaging 18 % of the HgT_{UNF} (Tables 2 and 3). $MeHgT_{UNF}$ were significantly higher below than above 100 m ($p<0.05$), suggesting removal and/or photodegradation for methylated Hg in upper layer and regeneration and/or production below (Fig. 4b, Table 2).

4.4. Deep profiles in the North Gyre

Summary statistics for Hg species concentrations are given in table 3. Methylated Hg concentrations in unfiltered samples ranged from 0.020 pmol L^{-1} at surface at Sta. S2400 to 0.478 pmol L^{-1} at 500 m at Sta. L-10 (Fig. 5a). Expressed as a fraction of the HgT, MeHgT varied between 16 to 30 % (Table 3). The $MeHgT_{UNF}$ profiles are typical of methylated Hg vertical distribution in open ocean (e.g., Fitzgerald et al., 2007; Cossa et al., 2011; Mason et al., 2012), i.e., very low concentrations at surface increasing with depth (Fig. 5a). At five stations, MMHg was determined in addition to MeHgT, allowing calculation of DMHg concentrations by difference. Results indicate MMHg/DMHg ratios always lower < 1, varying from 0.04 to 0.81 (Fig. 5b).

4.5. Sediment pore waters

Concentrations of $MeHgT_F$ in pore waters extracted from surface sediments (0-2 cm) were clearly higher (4-20 times) than in the overlaying waters and in the corresponding lower-water

column (Tables 3 and 4). Moreover, concentrations in sediment pore waters of North Gyre were one order of magnitude higher than the shelf pore waters, ranging from 2.05 to 2.18 pmol L^{-1} and from 0.07 to 0.68 pmol L^{-1}, respectively (Table 4).

4.6. *Ex situ* methylation experiments

Concentrations of inorganic Hg in sediments ranged from 0.432 ± 0.030 nmol g^{-1} (Sta. B) to 0.598 ± 0.122 nmol g^{-1} (Sta. A), with a mean of 0.519 ± 0.084 nmol g^{-1}. The results of the sediment incubation experiments showed clearly modified $MM^{199}Hg/MM^{200}Hg$ ratios compared to both natural values (0.72 ± 0.005; n = 3) and isotope ratios observed in control samples where incubation was stopped immediately after the spike (0.76 ± 0.023; n = 3; Fig. 6a). The three replicate incubations performed for each site generally provided reproducible results, revealing clear differences between the stations. The sediment samples from Sta. A ($MM^{199}Hg/MM^{200}Hg$ = 1.36 ± 0.06; n = 3) showed the highest methylation, whereas isotope ratios in the samples from Sta. B ($MM^{199}Hg/MM^{200}Hg$ = 0.85 ± 0.02; n = 3) were relatively close to natural values ($^{199}Hg/^{200}Hg$ = 0.73). Stations C ($MM^{199}Hg/MM^{200}Hg$ = 1.05 ± 0.11; n = 3) and D ($MM^{199}Hg/MM^{200}Hg$ = 1.11 ± 0.10; n = 3) showed intermediate and similar $MM^{199}Hg/MM^{200}Hg$, yet clearly different from control samples (Fig. 6a). From these isotope ratios, we estimated gross methylation rates between 0.009 and 0.083 % d^{-1} with means of 0.010 ± 0.001 % d^{-1} (Sta. B), 0.020 ± 0.005 % d^{-1} (Sta. C), 0.029 ± 0.010 % d^{-1} (Sta. D), and 0.059 ± 0.021 % d^{-1} (Sta. A). Incubations of unfiltered bottom water showed changing $MM^{199}Hg/MM^{200}Hg$ over time, reaching values of up to 8.7 after 192 h of incubation (n = 2, data not shown). The estimated methylation potentials for unfiltered bottom water ranged from 0.00019 % d^{-1} (after 48 h) to 0.00043 % d^{-1} (after 96 and 192 hours; Fig 6b).

5. DISCUSSION

5.1. External sources of MeHg

5.1.1. Advection from open sea

In the North Gyre, the $MeHgT_{UNF}$ concentrations varied from values below DL to 0.48 pmol L^{-1} (Table 3), which is similar in magnitude to those reported in the last ten years for the open Western Mediterranean waters (Cossa and Coquery, 2005; Kotnik et al., 2007; Cossa et al., 2009 and Heimbürger et al., 2010). The vertical MeHgT distribution patterns (Fig. 5) are consistent with the now classical oceanic MeHg behavioral model characterized by (i) a microbial net methylation within the oxycline, and (ii) a photodemethylation in surface waters. Photochemical demethylation is well documented in experimental and natural conditions (Suda et al., 1993; Black et al., 2012; Kim et al., 2016), whereas microbial methylation is supported by the occurrence of a peak of MeHg in the ODZs (e.g., Mason and Fitzgerald, 1990; Cossa et al., 2009; Sunderland et al., 2009). This model has recently been supported by isotopic Hg compositions observed in the waters of the Pacific Ocean (Blum et al., 2013). At stations L-10 and L-12, where water stratification was well established (Fig. S3), O_2-deficient Leventine Intermediate Water and maximum MeHgT concentrations were found between 200 and 400 m (Fig. 5a). For these two stations, and additionally Sta. M-10, statistically significant ($p<0.01$) relationships between MeHgT (pmol L^{-1}) and dissolved O_2 (µmol L^{-1}) exist (Fig. 7a), with similar regression coefficients, averaging -0.0063 ± 0.0001. For other stations, which comprise coastal sites (Stas. L-01, L-03 and M-12) and/or well mixed water column (Sta. S2400), the correlations were weak or inexistent. The corresponding average regression coefficient obtained for the relationships between MeHgT and apparent oxygen utilization (AOU) is +0.0059 ± 0.0007, which is close to the value

372 calculated for the whole Western Mediterranean (+0.0039, $R^2 = 0.77$, n = 40, according to
373 Cossa et al., 2009). In various parts of the World Ocean analogous distribution patterns have
374 been observed, showing undetectable methylated Hg concentrations in surface waters and
375 peaks deeper in the water column, where O_2 reaches a minimum due to organic carbon
376 remineralization (e.g., Mason and Fitzgerald, 1990; Cossa et al., 2009; Sunderland et al.,
377 2009; Cossa et al., 2011). According to the model, settling particulate organic carbon is both a
378 source of Hg^{II}_i to microbiologically-active waters and a source of organic matter to sustain
379 bacterial activity. A specific gene cluster is linked to Hg methylation in a variety of
380 microorganisms, including sulfate and iron-reducing bacteria and others (Park et al., 2013;
381 Gilmour et al., 2013).

382 Furthermore, we observed here more significant regression coefficient with a steeper
383 slope for the inverse relationship between DMHg and dissolved O_2 compared to that for
384 MMHg and dissolved O_2 (Fig. 7b), suggesting that the organic matter regeneration is more
385 directly connected to DMHg formation than MMHg formation. This fact is consistent with the
386 hypothesis proposed by Fitzgerald and Mason (1996) that MMHg in marine waters is not
387 formed directly, but is a degradation product of DMHg. The probability of this pathway is
388 reinforced by the observation that the highest MMHg/DMHg ratios occur during the
389 convection period (Fig. S3), when the O_2 depletion is limited and consequently net Hg
390 methylation is depressed (Fig. 5b). However, recent results (e.g., Jonsson et al., 2016;
391 Sorensen et al. 2016) leave the question of the Hg methylation pathway in the ocean open to
392 debate.

393 The Northern Current is the main source of waters for the Gulf of Lions. The horizontal
394 flux across the shelf-open sea boundary has been estimated to vary at different periods of the

year between 0.07 and 0.35 x 10^6 m^3 s^{-1} (Durrieu de Madron et al., 2003). The same authors also estimate a shelf—slope exchange as ~10 % of the along-slope transport, namely 0.2 x 10^6 m^3 s^{-1}. The chemical characteristics of waters entering the shelf are well represented by 0-100 m water layer found at Sta. Antarès. Using a $MeHgT_{UNF}$ mean concentration of 0.11 ± 0.02 pmol L^{-1} (n = 3), the MeHgT entering the shelf waters from the open sea *via* the Northern Current can be estimated as 680 ± 120 mol a^{-1}, representing 12 % of the HgT flux.

5.1.2. Atmospheric deposition

The MeHgT contribution from the atmospheric bulk wet deposition on the Gulf of Lions, based on results from section 4.1 and a surface area of the Gulf of 12 x 10^3 km^2, can be calculated as 2.5 ± 1.4 mol a^{-1}. In the absence of quantifiable analytical determinations, we assume a MeHgT dry deposition similar to the wet (as it is for the HgT in the Mediterranean environment according to Cossa and Coquery, 2005). Thus, the total MeHgT deposition into the waters of the Gulf of Lions can be estimated at ~5 mol a^{-1}, which is 2 % of the total HgT deposition.

5.1.3. Riverine and groundwater inputs

The amount of MeHgT transported annually by the Rhône River into the Gulf of Lions waters is estimated to be 5 mol a^{-1} for the dissolved phase and 51 mol a^{-1} for the particulate phase (see S1 2 for detailled calculation). Extrapolating these figures to transports from all the Gulf of Lions rivers gives a continental surface runoff contribution of 5.8 ± 2.0 and 59.7 ± 28.1 mol a^{-1}, for the dissolved and particulate MeHgT, respectively. The conservative mixing of dissolved MeHg between fresh and marine waters (Fig. 2a) allows an estimation of the annual net MeHgT efflux to the Gulf of Lions as equal to the gross efflux calculated above. Based on previous results, and owing to the fact that the Rhône River provides 85% and 83% all

418 riverine dissolved and solid discharges respectively (Gairoard et al., 2012), the total riverine
419 MeHg flux (dissolved + particulate) to the Gulf ranges within 53.3 - 77.7 mol a^{-1}, with a *99 %*
420 probability. At the scale of the Gulf of Lions, this mean flux is equivalent to ~ 10 % of the
421 MeHgT flux from marine source. To this surface runoff, the potential contribution of
422 groundwater should be added (Black et al. 2009b; Ganguli et al., 2012). In the absence of
423 direct measurement, a hypothetical estimate can be performed. Assuming values of
424 groundwater discharges to the Gulf of Lions of 2-30 % of the riverine discharge (Ollivier et
425 al., 2008), and MeHgT concentrations in groundwater similar to the only figures available to
426 date – i.e., those measured along the Southern Californian coasts (0.2-1.0 pmol L^{-1}, according
427 to Ganguli et al., 2012) –, we can approximate the MeHgT contribution of submarine
428 freshwater discharges to the Gulf of Lions waters to be in the range 0.2-17.4 mol a^{-1}. Given
429 the large uncertainties in this estimate, the MeHgT contribution from groundwater sources
430 remains to be assessed based on direct measurements. However, we can conclude that the
431 continental water contribution (gross efflux) is < 95 mol a^{-1} and small compared to open sea
432 (680 ± 120 mol a^{-1}) as a source of MeHgT for the Gulf of Lions.

433 ***5.13. Efflux from the shelf sediments***

434 The shelf sediments can be a source of MeHgT *via* the diffusion of soluble phase from
435 pore water across the sediment-water interface, *via* biopumping, and *via* the resuspension of
436 the surficial sediments during storm events. All these processes have not been determined,
437 however, in order to compare their magnitude with other MeHg sources, a "maximum
438 potential efflux" of MeHg from sediment has been estimated.

439 The pore-waters of the shelf surface sediments are MeHgT-enriched compared to the
440 overlying waters (Table 4). Using a simplified diffusion model (SI 3), we can calculate

potential diffusion effluxes from sediments varying from 0.2 to 2.6 pmol m^{-2} d^{-1} depending on the shelf stations and averaging 1.1 ± 0.8 pmol m^{-2} d^{-1} (n = 6). For the surface area of the Gulf of Lions shelf, which is 12 x 10^3 km^2, we estimate an annual potential diffusive flux of MeHgT from the sediment of 4.7 ± 3.5 mol, a figure similar to the dissolved riverine input (5.8 ± 2.0 mol a^{-1}). However, such a flux is not supported by MeHgT distribution in the water column of the shelf (Stas. A-E), since no vertical trend evoking a gradient near the bottom has been observed (Fig. 4a). In addition, a diffusive Hg flux out of the sediment may be counteracted by the presence of the oxic layer near the sediment surface, where upward diffusing Hg species may be trapped (Muresan et al. 2007). On the continental shelf of the Gulf of Lions, oxygen penetration depth in the sediments increases with water depth and distance from shore (Pruski et al, 2015). Oxidised conditions can be restricted from some millimeters to some centimeters in the proximal Rhône (20-30 m), extended down to 2-5 cm at 60 m depth (Table 4) and to 5-10 cm offshore at 100 m depth. In the sediment cores collected on the Gulf of Lions shelf during the CASCADE cruise, an oxic layer was always present at the benthic interface (Table 4). This layer should act as an efficient barrier for upward diffusion of the pore water $MeHgT_F$, by adsorption onto oxyhydroxides ($\log Kd_{MeHg}$ equal to 6.4 and 7.7 for FeO_x and MnO_x, respectively, according to Muresan et al., 2007) or onto organic matter associated with oxides according to the model by Feyte et al. (2010).

If diffusion of MeHgT from sediments is unlikely, MeHg advection from sediment *via* bioirrigation and biopumping is more probable. Assuming this advective flux to be 3 times the diffusion flux, as calculated by Hammerschmidt and Fitzgerald (2008) for the Northeastern Atlantic coastal sediments, the biomediated MeHg efflux from sediments would be ~14.1 mol a^{-1}.

Release of porewater-borne MeHgT during resuspension of surface sediment is an alternative methylated Hg source for shelf waters. Assuming a 2-cm thick layer (with a mean porosity of 0.82, according to Cathalot et al., 2010) of MeHgT-enriched pore water resuspended (0.3 ± 0.2 pmol L^{-1} according to Table 4) and 12 x 10^3 km^2 for the Gulf of Lions shelf surface area, the quantity of MeHgT mobilized at each storm event would be 0.07 ± 0.05 mol. According to Guizien (2009) the magnitude of the period with waves higher than 1.5 m on the Gulf of Lions shelf is around 10 % of the year. This means that a maximum of 37 days of resuspension (i.e., ~ fifteen 2.5 days-long storm events, Bourrin et al., 2012; Dumas et al., 2014) can be estimated leading to the annual injection of 2.7 ± 1.9 mol of MeHgT in the water column. Thus, the "maximum potential efflux" of MeHg from the shelf sediment of the Gulf of Lions would be ~16.8 mol a^{-1}. Of course, factors such as demethylation at the sediment–water interface as well as MeHg readsorption on resuspended particles may reduce this figure. It is noteworthy that this "maximum potential efflux" is equivalent to 2.5 % of the methylated Hg entering the Gulf of Lions from the sea and 28 % of the riverine particulate MeHgT flux, from which it partialy derives.

5.2. Internal MeHg production

5.2.1. Shelf and slope waters

The average of $MeHgT_F$ concentrations in the Low Salinity Waters was low (< 0.05 pmol L^{-1}) and not different from the rest of the Gulf of Lions shelf waters (*t*-test, $p > 0.01$, Tables 2 and 3). The average $MeHgT_F$ / HgT_F ratio was 1.5 %. These low levels are consistent with active photodemethylation in the surface waters (e.g., Black et al., 2012). The highest $MeHgT_F$ concentrations occurred where highest salinities were present at the bottom of the Low Salinity Waters lenses (Fig. 2b, Fig. 3), suggesting two possible origins for methylated Hg: its

advection from the external sources quantified above (Northern Current waters and shelf sediment) and/or its production in the shelf water column. Methylated Hg production associated with planktonic production/degradation in the mixed layer has been shown already in the Mediterranean Sea (Monperrus et al., 2007; Heimbürger et al., 2010) and elsewhere (e.g., Lehnherr et al., 2011).

In the surface waters of the Low Salinity Waters, significant relationships exist between $MeHgT_P$ and particulate phosphorus ($MeHgT_{P pmol\ L^{-1}} = 0.0723 P_{P \mu mol\ L^{-1}} - 0.0048$, $R^2 = 0.44$, $0.01<p<0.05$, Fig. S4a), and between $MeHgT_P$ and total pigments ($MeHgT_{P pmol\ L^{-1}} = 0.0044 Pig_{\mu g\ L^{-1}} - 0.0078$, $R^2 = 0.43$, $0.01<p<0.05$, Fig. S4b). This relationship suggests methylated Hg accumulation in the phytoplankton of the Low Salinity Waters; however, its origin is unidentified. Interestingly, $MeHgT_P$ is significantly inversely correlated with the $MeHgT_F$ in Low Salinity Water surface waters ($MeHgT_{F pmol\ L^{-1}} = - 0.600 MeHgT_{P pmol\ L^{-1}} + 0.030$, $R^2 = 0.46$, $p<0.05$, Fig. S5). With a regression coefficient not different from 1 (-0.600 ± 0.415; $p = 0.05$), this relationship suggests that the two phases were exchanging the MeHgT standing stock present in the water.

Along the slope (Sta. S230), $MeHgT_{UNF}$ distribution is related to soluble reactive phosphorus (SRP) with the following relationship: $MeHgT_{UNF pmol\ L^{-1}} = 0.92 SRP_{\mu mol\ L^{-1}} + 0.04$ ($R^2 = 0.95$, $p<0.01$). The regression coefficient is in the range of values reported for open Mediterranean waters, namely 0.89 to 1.24 (see Table 2 in Cossa et al., 2009). These values calculated for unfiltered samples are more than 10 times higher than the regression coefficient for the relationship between $MeHg_P$ and P_P mentioned above (0.0723). If the mineralization of settling particules were responsible for the $MeHg_F$ *versus* SRP relationship, similar regression coefficients should be found for the particulate and the dissolved phases. On the other hand,

the discrepancy in the regression coefficients between $MeHg_F$ *vs* SRP and $MeHg_P$ *vs* P_P suggests that MeHg-enriched water is advected with Northern Current and/or that net Hg methylation occurs in the organic matter regeneration zone of the slope water column. The significant increase in MeHgT concentrations in the slope waters when dissolved oxygen decreases ($R^2 = 0.90$; n = 21, $p<0.01$) supports this latter interpretation (Fig. S6).

In summary, net Hg methylation seems to occur along the slope water column, whereas we find little evidence for it to occur in the Low Salinity Water lenses drifting on the Gulf of Lions shelf. This observation probably indicates that particulate organic matter degradation, which governs the Hg^{II}_i methylation, is favored when the water column is deep enough to sustain a sufficiently long residence time of settling particles. In contrast, on the shelf, where the water column depth is limited, organic matter degradation mostly occurs in the surface sediments. Incubation experiments allowed estimating the Hg methylation potentials within the Gulf of Lions water and sediment.

5.2.2. In situ *Hg methylation potential*

Week-long (192 h) incubation experiments suggest gross Hg methylation t rates of 0.009 to 0.083 % d^{-1} during sediment resuspension. In addition, incubations of bottom seawater sampled on the shelf during winter downwelling gave Hg methylation potentials (over 192 h) ranging from 0.0002 to 0.0004 % d^{-1}. Interestingly, the methylation rates increased during the first 96 h of incubation then remained constant at the maximum level after 96 to 192 h (Fig. 6b). Applying the above methylation potentials to the flux of inorganic particulate Hg calculated from the mean concentration of inorganic particulate Hg measured in March 2011 in the Gulf of Lions (0.519 nmol g^{-1}) and the downwelling mass flux of 0.4 x 10^{12} g per storm event (2-3 days-long; Bourrin et al., 2012; Dumas et al., 2014), the gross methylation

533 observed in sediment slurries may account at best for 0.02 to 0.17 mol.d^{-1} MeHgT (i.e. 0.05-
534 0.42 mol MeHgT per storm event), that is 0.7 to 6.3 mol per year for 15 storms a year. These
535 considerations suggest that the contribution of MeHgT produced in sediment slurries resulting
536 from sediment resuspension in bottom water and short-term settling/resuspension cycles may
537 be similar in magnitude to MeHgT release from porewater (2.7 mol a^{-1}). If we apply the gross
538 methylation rates obtained in bottom water (up to 0.0004 % d^{-1}) to the whole water column
539 (with a Hg^{II}_i of 0.85 pmol L^{-1}), the maximum methylation rate in the entire Gulf of Lions
540 waters (~1.8 x 10^3 km^3) should not exceed 2.2 mol a^{-1}.

541

542 **6. SUMMARY AND CONCLUSIONS**

543 Reviewing the oceanic Hg biogeochemical cycle, Mason et al. (2012) sum up that, while
544 atmospheric deposition is the main source of inorganic divalent Hg in open ocean systems,
545 most of the MMHg accumulating in ocean fish should derive from *in situ* production in the
546 upper water column. Is this model proposed for the open seas also valid for the coastal
547 environment? Here, we have addressed the questions of the distribution and sources of
548 methylated Hg in the waters of the Northwestern Mediterranean margin including the
549 continental shelf (Gulf of Lions) and the adjacent open sea (North Gyre). In summary, it
550 appears that the proportion of methylated Hg to HgT increased seaward, from the freshwaters
551 (Rhône River waters) to the shelf waters (Gulf of Lions waters) and the open ocean (North
552 Gyre waters). Highest MeHgT concentrations are associated with the ODZs of the North
553 Gyre. Despite the observed *in situ* methylation of inorganic Hg in sediment and waters within
554 the system (<6.3 and ~2.2 mol a^{-1}, respectively), external methylated Hg sources are the
555 largest for the Gulf of Lions. The adjacent open ocean is the dominant source, with 680 ± 120

556 mol of MeHg per year. Continental sources (river and groundwater) account for < 95 mol a^{-1},
557 with MeHg being mainly associated with continental particulate matter, a phase which is not
558 directly available for pelagic biota. Contributions from atmospheric deposition and sediment
559 resuspension are estimated to be ~5 and <16.8 mol a^{-1}, respectively. We conclude that (i) the
560 methylation of inorganic Hg in the ODZs of the open sea is the main source of methylated Hg
561 in the Northwestern Mediterranean margin waters, and that (ii) sedimentary sources have a
562 lower influence on the distribution of MeHgT in the water column, even though high
563 methylated Hg concentrations in the sediments may cause the exposure of organisms feeding
564 on food webs linked to the benthic environment. Our findings underline the ecological
565 importance of the idea that, even in coastal contaminated environments, methylated Hg
566 transfer into food webs is driven by the efficiency of processes that determine MeHgT inputs
567 to the water column (Sunderland et al., 2010; Chen et al., 2014). We are in favor of an
568 approach where, in coastal ecosystems, the origin of MeHg accumulated through pelagic and
569 benthic food webs are differentiated using stable Hg isotopes (Mason et al., 2012).

570

571 **Acknowledgments:** Thanks are due to Bernard Averty, Jean-François Chiffoleau, Nicole
572 Garcia, Christine Sotin and Roger Kerouel who participated to sampling or analytical works
573 and to captains and crews of R/V SUROIT (BIOPRHOFI cruise) and R/V ATALANTE (CASCADE
574 cruise). Special thank to François Dufois for his helpful comments and to Mac Vautour for
575 editing the English. The manuscript was greatly improved by numerous comments of one
576 refeer and the associated editor. This research received funding from the French National
577 Research Agency (EXTREMA project, N° ANR-06-VULN-005), and the European
578 Commission's Seventh Program (HERMIONE project, N° 226354), the Région Aquitaine

579 (FEDER Aquitaine-1999-Z0061) and the MERMEX / MISTRALS project. It is a contribution
580 to the international LOICZ program.
581

582
583 **References**

584 Aminot A. and Kérouel K. (2007) *Dosage automatique des nutriments dans les eaux marines:*
585 *méthodes en flux continu.* Méthodes d'analyse en milieu marin. Editions Quae. 187 pages.
586 ISBN 978-2-7592-0023-8.

587 Balcom P. H., Hammerschmid C. R., Fitzgerald W. F., Lamborg C. H. and O'Connor J. S.
588 (2008) Seasonal distributions and cycling of mercury and methylmercury in the waters of
589 New York/New Jersey Harbor Estuary. *Mar. Chem.,* **109**, 1-17.

590 Balcom P. H., Schartup A. T., Mason R. P. and Chen C. Y. (2015) Sources of water column
591 methylmercury acrossmultiple estuaries in the Northeast U.S. *Mar. Chem*., **177**, 721–730.

592 Barnett P.R.O., Watson J. and Connelly D. (1984) A multiple corer for taking virtually
593 undisturbed samples from shelf, bathyal and abyssal sediments. *Oceanol. Acta*, **7**, 399-408.

594 Black F. J., Conaway C. H. and Flegal A. R. (2009a) Stability of Dimethyl Mercury in
595 Seawater and Its Conversion to Monomethyl Mercury. *Environ. Sci. Technol*., **43**, 4056-
596 4062.

597 Black F. J., Paytan A., Knee K. L., de Sieyes N. R., Ganguli P. M., Gray E. and Flegal A. R.
598 (2009b) Submarine Groundwater Discharge of Total Mercury and Monomethylmercury to
599 Central California Coastal Waters. *Environ. Sci. Technol.*, **43**, 5652-5659.

600 Black F. J., Poulain B. A. and Flegal A. R. (2012) Factors controlling the abiotic photo-
601 degradation of monomethylmercury in surface waters. *Geochim. Cosmochim. Acta*, **84**,
602 492-507.

603 Blum J. D., Popp B. N., Drazen J., Choy C. A. and Johnson M. W. (2013) Methylmercury
604 production below the mixed layer in the North Pacific Ocean. *Nature Geosci.*, **6**, 879-884.

605 Bourrin F., Durrieu de Madron X., Mahiouz K., Guery L. B. and Houpert L. (2012) Sediment
606 resuspension observed by an optical slocum glider during a typical Mediterranean winter
607 storm. Ocean Science Meeting 2012, Salt Lake City, USA.

608 Bourrin F., Many G., Durrieu de Madron X., Martín J., Puig P., Houpert L., Testor P.,
609 Kunesch S., Mahiouz K. and Béguery L. (2015) Glider monitoring of shelf suspended

particle dynamics and transport during storm and flooding conditions. *Cont. Shelf Res*., **109**, 135-49.

Bowman K. L., Hammerschmidt C. R., Lamborg C. H. and Swarr G. (2015) Mercury in the North Atlantic Ocean: The U.S. GEOTRACES zonal and meridional sections. *Deep Sea Res. II*, **116**, 251-261.

Bradley P. M., Burns D. A., Riva-Murray K., Brigham M. E., Button D. T., Chasar L. C., Marvin-DiPasquale M., Lowery M. A. and Journey C. A. (2011) Spatial and Seasonal Variability of Dissolved Methylmercury in Two Stream Basins in the Eastern United States. *Environ Sci. Technol*., **45**, 2048-2055.

Buck C. S., Hammerschmidt C. R., Bowman K. L., Gill G. A. and Landing W. M. (2015) Flux of Total Mercury and Methylmercury to the Northern Gulf of Mexico from U.S. Estuaries. *Environ. Sci. Technol*., **49**, 13992-13999.

Castelle S. (2010) Suivi des apports en mercure au Golfe du Lion par voies atmosphérique et fluvial. Rapport Ifremer N° RST.DOP/BE /LBCM/025.

Cathalot C., Rabouille, Pastor L., Deflandre B., Viollier E., Buscail R., Grémare A., Treignier C. and Pruski A. (2010) Temporal variability of carbon recycling in coastal sediments influenced by rivers: assessing the impact of flood inputs in the Rhône River prodelta. *Biogeosciences*, **7**, 1187-1205.

Charmasson S., Radakovitch O., Arnaud M., Bouisset P. and Pruchon A. S. (1998) Long-core profiles of ^{137}Cs, ^{134}Cs, ^{60}Co and ^{210}Pb in sediment near the Rhône river (Northwestern Mediterranean Sea). *Estuaries*, **21**, 367-378.

Chen C. Y., Borsuk M. E., Bugge D. M., T. Hollweg D. M., Balcom P. H., Ward D. M., Williams J. and Mason R. P. (2014) Benthic and Pelagic Pathways of Methylmercury Bioaccumulation in Estuarine Food Webs of the Northeast United States. *Plos One*, **9**, Issue 2, e89305, p.1-11.

Choe K.-Y. and Gill G. A. (2003) Distribution of particulate, colloidal, and dissolved mercury in San Francisco Bay estuary. 2. Monomethyl mercury. *Limnol. Oceanogr*., **48**, 1547-1556.

Clarkson T. W. and Magos L. (2006) The toxicology of mercury and Clarkson its chemical compounds. *Crit Rev Toxicol*., **36**, 609-662.

639 Conaway C. H., Black F. J., Gault-Ringold M., Pennington J. T., Chavez F. P. and Flegal A.
640 R. (2009) Dimethylmercury in coastal upwelling waters, Monterey Bay, California.
641 *Environ. Sci. Technol*., **43**,1305-1309.

642 Coquery M., Cossa D. and Sanjuan J. (1997) Speciation and Sorption of Mercury in Two
643 Macro-Tidal Estuaries. *Mar. Chem*., **58**, 213-227.

644 Cossa D., Martin J.-M. and Sanjuan J. (1994) Dimethylmercury formation in the Alboran Sea.
645 *Mar. Poll. Bull.*, **28**, 381-384.

646 Cossa D., Coquery M., Gobeil C. and Martin J.-M. (1996) Mercury Fluxes at the Ocean
647 Margins. 229-247. In: *Regional and Global Cycles of Mercury: Sources, Fluxes, and Mass*
648 *Balances*. W. Baeyens, R. Ebinghaus and O. Vasiliev éditeurs. Kluwer Academic
649 Publishers, Dordrecht, The Netherlands.

650 Cossa D., Martin J.-M., Takayanagi K. and Sanjuan J. (1997) The Distribution and Cycling of
651 Mercury in the Western Mediterranean. *Deep Sea Res. II,* **44**, 721-740.

652 Cossa D., Averty B., Breaudeau J. and Senard A.-S. (2003) *Spéciation du mercure dissous*
653 *dans les eaux marines. Analytical methods for the marine environments*. Ifremer and
654 French Ministry for Ecology and Sustainable Development publication MA0303.

655 Cossa D. and Coquery M. (2005) The Mediterranean mercury anomaly, a geochemical or a
656 biological issue. pp 177-208. In: *The Mediterranean Sea*. Handbook of Environmental
657 Chemistry, Vol 5. Saliot, A. editeur. Springer, 413 p. ISSN 1433-6863.

658 Cossa D., Averty B. and Pirrone N. (2009) The origin of methylmercury in open
659 Mediterranean waters. *Limnol. Oceanogr.,* **54**, 837-844.

660 Cossa D., Heimbürger L.-E., Lannuzel D., Rintoul S. R., Butler E. C. V., Bowie A. R., Averty
661 B., Watson R. J. and Remenyi T. (2011) Mercury in the Southern Ocean. *Geochim.*
662 *Cosmochim. Acta,* **75**, 4037-4052.

663 Dumas C., Aubert D., Durrieu de Madron X., Ludwig W., Heussner S., Delsaut N., Menniti
664 C., Sotin C. and Buscail R. (2014) Storm-Induced transfer of particulate trace metals to the
665 deep-sea in the Gulf of Lion (NW Mediterranean Sea). *Environ. Geochem. Health*, **36**,
666 995-1014.

667 Durrieu de Madron X., Denis L., Diaz F., Garcia N., Guieu C., Grenz C., Loÿe-Pilot M.-D.,
668 Ludwig W., Moutin T., Raimbault P. and Ridame C. (2003) Nutrients and carbon budgets
669 for the Gulf of Lion during the Moogli cruises. *Oceanol. Acta*, **26**, 421-433.

670 Durrieu de Madron X., Wiberg P. L. and Puig P. (2008) Sediment dynamics in the Gulf of
671 Lions: The impact of extreme events. *Cont. Shelf Res.*, **28**, 1867-1876.

672 Elbaz-Poulichet F., Garnier J.-M., Guan D. M., Martin J.-M. and Thomas A. J. (1996) The
673 conservative behaviour of trace metals (Cd, Cu, Ni and Pb) and as in the surface plume of
674 stratified estuaries: Example of the Rhône river (France). *Estuar. Coast. Shelf Sci*., **42**, 289-
675 310.

676 Feyte S., Tessier A., Gobeil C. and Cossa D. (2010) In situ adsorption of mercury,
677 methylmercury and other elements by iron oxyhydroxides and organic matter in lake
678 sediments. *Appl. Geochem*., **25**, 984-995.

679 Fitzgerald W. F. and Mason R. P. (1996) The global mercury cycle: oceanic and
680 anthropogenic aspects. 85- 108. In: *Regional and Global Cycles of Mercury: Sources,*
681 *Fluxes, and Mass Balances*. W. Baeyens, R. Ebinghaus and O. Vasiliev éditeurs. Kluwer
682 Academic Publishers, Dordrecht, The Netherlands.

683 Fitzgerald W. F., Lamborg C. H. and Hammerschmidt C. R. (2007) Marine biogeochemical
684 cycling of mercury. *Chem. Rev.,* **107**, 641-662.

685 Ganguli P. M., Conaway C. H., Swarzenski P. W., Izbicki J. A. and Flegal A. R. (2012)
686 Mercury Speciation and Transport via Submarine Groundwater Discharge at a Southern
687 California Coastal Lagoon System. *Environ. Sci. Technol*., **46**, 1480-1488.

688 Gilmour C. C., Podar M., Bullock A. L., Graham A. M., Brown S. D., Somenahally A. C.,
689 Johs A., Hurt R. A., Bailey K. L. and Elias D. A. (2013) Mercury Methylation by Novel
690 Microorganisms from New Environments. *Environ. Sci. Technol*., **47**, 11810-11820.

691 Gobeil C. and Cossa D. (1993) Mercury in the sediments and sediment pore waters in the
692 Laurentian trough. *Can. J. Fish. Aquat. Sci.,* **50**, 1794-1800.

693 Guédron S., Huguet L., Vignati D. A. L., Liu B., Gimbert F., Ferrarin B. J. D., Zonta R.and
694 Dominik J. (2012) Tidal cycling of mercury and methylmercury between sediments and
695 water column in the Venice Lagoon (Italy). *Mar. Chem*., **130-131**, 1-11.

696 Guizien K. (2009) Spatial Variability of Wave Conditions in the Gulf of Lions (NW
697 Mediterranean Sea). *Vie et Milieu-Life and Environment*, **59**, 261-270.

698 Hammerschmidt C. R., Fitzgerald W. F., Lamborg C. H., Balcom P. H. and Visscher P. T.
699 (2004) Biogeochemistry of methylmercury in sediments of Long Island Sound. *Mar.*
700 *Chem.*, **90**, 31-52.

701 Hammerschmidt C. R. and Fitzgerald W. F. (2006) Methylmercury cycling in sediments on
702 the continental shelf of southern New England**.** *Geochim. Cosmochim. Acta,* **70**, 918-930.

703 Hammerschmidt C. R., Lamborg C. H. and Fitzgerald W. F. (2007) Aqueous phase
704 methylation as a potential source of methylmercury in wet deposition. *Atmos. Environ*., **41**,
705 1663-1668.

706 Hammerschmidt C. R. and Bowman K. L. (2012) Vertical methylmercury distribution in the
707 subtropical North Pacific Ocean. *Mar. Chem*., **132-133**, 77-82.

708 Hedges J. I. and Stem J. H. (1984) Carbon and nitrogen determinations of carbonate-
709 containing solids. *Limnol. Oceanogr*., **29**, 663-666.

710 Heimbürger L.-E., Cossa D., Marty J.-C., Migon C., Averty B., Dufour A. and Ras J. (2010)
711 Methyl mercury distributions in relation to the presence of nano and picophytoplankton in
712 an oceanic water column (Ligurian Sea, North-western Mediterranean). *Geochim.*
713 *Cosmochim. Acta,* **74**, 5549-4459.

714 Hollweg T. A., Gilmour C. C. and Mason R. P. (2009) Methylmercury production in
715 sediments of Chesapeake Bay and the mid-Atlantic continental margin. *Mar. Chem*. **114**,
716 86-101.

717 Hollweg T. A., Gilmour C. C. and Mason R. P. (2010) Mercury and methylmercury cycling in
718 sediments of the mid-Atlantic continental shelf and slope. *Limnol. Oceanogr*., **55**, 2703-
719 2722.

720 Horvat M., Liang L., Azemard S., Mandić V., Villeneuve J.-P. and Coquery M. (1997)
721 Certification of total mercury and methylmercury concentrations in mussel homogenate
722 (*Mytilus edulis*) reference material, IAEA-142. *Fresenius J. Anal. Chem.,* **358**, 411-418.

723 Horvat M., Kotnik J., Logar M., Fajon V., Zvonaric T. and Pirrone N. (2003) Speciation of
724 mercury in surface and deep-sea waters in the Mediterranean Sea. 2003. *Atmos. Environ.*,
725 **37**, S93-S108.

726 Huguet L., Castelle S., Schäfer J., Blanc G., Reynouard C. and Jorand F. (2010) Mercury
727 methylation rates of biofilm and plankton microorganisms from a hydroelectric reservoir in
728 French Guiana. *Sci. Total Environ.,* **408**, 1338-1348.

729 Jensen S. and Jernelöv A. (1969) Biological methylation of mercury in aquatic organisms.
730 *Nature (Lond.),* **223**, 753-754.

731 Jonsson S., Mazrui N. M. and Mason R. P. (2016) Dimethylmercury Formation Mediated by
732 Inorganic and Organic Reduced Sulfur Surfaces. *Sci. Rep*., **6**, 27958; doi:
733 10.1038/srep27958.

734 Kim, M-K., Won, A-Y. and Zoh, K-D. (2016) The production of dissolved gaseous
735 mercury from methylmercury photodegradation at different salinity. *Desal. Wat.*
736 *Treat*., **57**, 610-619.

737 Kotnik J., Horvat M., Tessier E., Ogrinc N., Monperrus M., Amouroux D., Fajon V., Gibičar
738 D., Žižek S., Sprovieri F. and Pirrone N. (2007) Mercury speciation in surface and deep
739 waters of the Mediterranean Sea. *Mar. Chem*., **107**, 13- 30.

740 Lehnherr I., St. Louis V. L., Hintelmann H. and Kirk J. L. (2011) Methylation of inorganic
741 mercury in polar marine waters. *Nature Geosci*., **4**, 298-302.

742 Lehnherr I. (2014) Methylmercury biogeochemistry: a review with special reference to Arctic
743 aquatic ecosystems. *Environ. Rev*. **22**, 229on. dx.doi.org/10.1139/er-2013-0059.

744 Liang L., Horvat M. and Bloom N. S. (1994) An improved speciation method for mercury by
745 GC/CVAFS after aqueous phase ethylation and room temperature precollection. *Talanta*,
746 **41**, 371-379.

747 Luengen A. C. and Flegal A. R. (2009) Role of phytoplankton in mercury cycling in the San
748 Francisco Bay estuary. *Limnol. Oceanogr*., **54**, 23-40.

749 Maillet G. M., Vella C., Berné S., Friend P. L., Amos C. L., Fleury T. J. and Normand A.
750 (2006) Morphological changes and sedimentary processes induced by the December 2003

751 flood event at the present mouth of the Grand Rhône River (southern France). *Mar. Geol.,*
752 **234**, 159-177.

753 Marion C., Dufois F., Arnaud M. and Vella C. (2010) In situ record of sedimentary processes
754 near the Rhône River mouth during winter events (Gulf of Lions, Mediterranean Sea).
755 *Cont. Shelf Res.*, **30**, 1095-1107.

756 Marusczak N., Larose C., Dommergue A., Yumvihoze E., Lean D., Nedjai R. and Ferrarri C.
757 (2011) Total mercury and methylmercury in high altitude surface snow from the French
758 Alps. *Sci. Total Environ*., **409**, 3949-3954.

759 Marusczak N., Castelle S, de Vogüé B, Knoery J. and Cossa D. (2015) Seasonal Variations of
760 Total Gaseous Mercury at a French Coastal Mediterranean Site. *Aerosol and Air Quality*
761 *Research*, doi:10.4209/aaqr.2015.04.0219.

762 Mason R. P. (1991) *The chemistry of mercury in the equatorial Pacific Ocean*. PhD Thesis.
763 University of Connecticut, USA, 305 pp.

764 Mason R. P. and Fitzgerald W. F. (1990) Alkylmercury species in the equatorial Pacific.
765 *Nature (Lond.)*, **347**, 457-459.

766 Mason R. P., Fitzgerald W. F., Hurley J. P., Hanson A. K., Donaghay P. L. and Sieburth J. M.
767 (1993) Mercury biogeochemical cycling in a stratified estuary. *Limnol. Oceanogr*., **38**,
768 1227-1241.

769 Mason R. P., Rolfhus K. R. and Fitzgerald W. F. (1998) Mercury in the North Atlantic *Mar.*
770 *Chem.,* **61**, 37-53.

771 Mason R. P. and Sullivan K. A. (1999) The distribution and speciation of mercury in the
772 South and equatorial Atlantic. *Deep-Sea Res. II,* **46**, 937-956.

773 Mason R. P., Choi A. L., Fitzgerald W. F., Hammerschmidt C. R., Lamborg C. H., Soerensen
774 A. L. and Sunderland E. M. (2012) Mercury biogeochemical cycling in the ocean and
775 policy implications. *Environ. Res.,* **119**, 101-117.

776 Millot C. and Taupier-Letage I. (2005) *Circulation in the Mediterranean Sea*, p. 29-66. In:
777 *The Mediterranean Sea*. Handbook of Environmental Chemistry, Vol 5. Saliot, A. editeur.
778 Springer, 413 p. ISSN 1433-6863.

779 Monperrus M. (2004) Utilisation de traceurs isotopiques stables pour la spéciation du mercure
780 et des butylétains : Application à l'étude de la biométhylation du mercure dans les
781 environnements aquatiques. PhD Thesis. Université de Pau et Pays de l'Adour, France.

782 Monperrus M., Tessier E., Amouroux D., Leynaert A., Huonnic P. and Donard O. F. X.
783 (2007) Mercury methylation, demethylation and reduction rates in coastal and marine
784 surface waters of the Mediterranean Sea. *Mar. Chem*., **107,** 49-63.

785 Morel A. and André J.-M. (1991) Pigment distribution and primary production in the western
786 Mediterranean as derived and modeled from coastal zone color scanner observations. *J.*
787 *Geophys. Res. (Oceans)*, **96**, 12685-12698.

788 Munson K. M., Lamborg C. H., Swarr G. J.and Saito M. A. (2015) Mercury Species
789 concentrations and fluxes in the Central Tropical Pacific Ocean. *Global Biogeochem.*
790 *Cycle*, doi:10.1002/2015GB005120. 1-21p.

791 Muresan B., Cossa, D. Jézéquel D., Prévot F. and Kerbellec S. (2007) The biogeochemistry of
792 mercury at the sediment water interface in the Thau lagoon. 1. Partition and speciation.
793 *Estuar. Coast. Shelf Sci.*, **72**, 472-484.

794 Muresan B., Cossa D., Coquery M. and Richard S. (2008) Mercury sources and
795 transformations in a man-perturbed tidal estuary: The Sinnamary Estuary, French Guiana.
796 *Geochim. Cosmochim. Acta*, **72**, 5416-5430.

797 Murphy J. and Riley J. P. (1962) A modified single solution methode for the determination of
798 phosphates in natural waters. *Anal. Chem. Acta*, **27**, 31-36.

799 Naudin J.-J., Cauwet G., Chrétiennot-Dinet M.-J., Deniaux B., Devenon J.-L. and Pauc H.
800 (1997) River discharges and wind influence upon particulate transfer at the land-ocean
801 interaction: case study of the Rhône River plume. *Estuar. Coast. Shelf Sci*., **45**, 303-316.

802 Noh S., Choi M., Kim E., Dan N. P., Thanh B. X., Van Ha N. T., Sthiannopkao S. and Han S.
803 (2013) Influence of salinity intrusion on the speciation and partitioning of mercury in the
804 Mekong River Delta. *Geochim. Cosmochim. Acta,* **106**, 379-390.

805 Ollivier P., Claude C., Radakovitch O. and Hamelin B. (2008) TIMS measurements of ^{226}Ra
806 and ^{228}Ra in the Gulf of Lion, an attempt to quantify submarine groundwater discharge.
807 *Mar. Chem.,* **109**, 337-354.

808 Ormaza-Gonzales F. I. and Statham P. J. (1996) A comparison of methods for the
809 determination of dissolved and particulate phosphorus in natural waters. *Water Res*., **30**,
810 2739-2747.

811 Ortiz V., Mason R. P.and Ward J. E. (2015) An examination of the factors influencing
812 mercury and methylmercury particulate distributions, methylation and demethylation rates
813 in laboratory-generated marine snow. *Mar. Chem*., **177**, 753-762.

814 Parks J. M., Joh A., Podar M., Bridou R., Hurt R. A., Smith S. D., Tomanicek S. J., Qian Y.,
815 Brown S. D., Brandt C. C., Palumbo A. V., Smith J. C., Wall J. D., Elias D. A. and Liang
816 L. (2013) The Genetic Basis for Bacterial Mercury methylation. *Science*, **339**, 1332-1335.

817 Pruski A. M., Buscail R., Bourgeois S., Vétion G., Coston-Guarini J. and Rabouille C. (2015)
818 Biogeochemistry of fatty acids in a river-dominated Mediterranean ecosystem (Rhône
819 River prodelta, Gulf of Lions, France): Origins and diagenesis. *Org. Geochem.,* **83-84**,
820 227-240.

821 Radakovitch O., Charmasson S., Arnaud M. and Bouisset P. (1999) Pb-210 and caesium
822 accumulation in the Rhône delta sediments. *Estuar. Coast. Shelf Sci.,* **48**, 77-92.
823 doi:10.1006/ecss.1998.0405.

824 Schartup A. T., Balcom P. H., Soerensen A. L., Gosnellc K. J., Calder R. S. D., Mason R. P.
825 and Sunderland E. M. (2015) Freshwater discharges drive high levels of methylmercury in
826 Arctic marine biota. *PNAS*, doi/10.1073/pnas.1505541112.

827 Sorensen A. L., Jacob D. J., Schartup A. T., Fisher J., Lehnherr I., St. Louis V., Heimbürger
828 L.-E., Sonke J. E., Krabbenhoft D. P. and Sunderland E.M. (2016) A mass budget for
829 mercury and methylmercury in the Arctic Ocean. Global Biogeochem. Cycles,
830 doi:10.1002/2015GB005280.

831 Stoichev T. R., Rodriguez Martin-Doimeadios C., Tessier E., Amouroux D. and Donard O. F.
832 X. (2004) Improvement of analytical performances for mercury speciation by on-line
833 derivatization, cryofocussing and atomic fluorescence spectrometry. *Talanta,* **62**, 433-438.

834 Strickland J. D. H. and Parsons T. R. (1972) A Practical Handbook of Seawater Analysis.
835 *Bull, Fish. Res. Board Can*., **167**, 311 pp.

836 Suda I., Suda M., and Hirayama K. (1993) Degradation of methyl and ethyl mercury by
837 singlet oxygen generated from sea water exposed to sunlight or ultraviolet light. *Arch.*
838 *Toxicol*., **67**, 365-368.

839 Sunderland E. M., Krabbenhoft D. P., Moreau J. W., Strode S. A. and Landing W. M. (2009)
840 Mercury sources, distribution, and bioavailability in the North Pacific Ocean: Insights from
841 data and models. *Global Biogeochem. Cycles,* **23**, GB2010, doi:10.1029/2008GB003425.

842 Sunderland E. M., Dalziel J., Heyes A., Branfireun B. A., Krabbenhoft D. P. and Gobas F. A.
843 C. P. (2010) Response of a Macrotidal Estuary to Changes in Anthropogenic Mercury
844 Loading between 1850 and 2000. *Environ. Sci. Technol.,* **44**, 1698-1704.

845 Ulses C., Estournel C., Durrieu de Madron X. and Palanques A. (2008) Sediment transport in
846 the Gulf of Lion (NW Mediterranean): Impact of extreme storms and floods. *Cont. Shelf*
847 *Res.*, **28,** 2048-2070.

848 Wang F., Macdonald R. W., Armstrong D. A. and Stern G. A. (2012) Total and Methylated
849 Mercury in the Beaufort Sea: The Role of Local and Recent Organic Remineralization.
850 *Environ. Sci. Technol.,* **46**, 11821-11828.

851 Weiss-Penzias P. S., Ortiz C. Jr., Acosta R. P., Heim W., Ryan J. P., Fernandez D., Collett J.
852 L. Jr. and Flegal A. R. (2012) Total and monomethyl mercury in fog water from the central
853 California coast. *Geophys. Res. Lett*., **39**, L03804, doi:10.1029/2011GL050324, 2012

854 Weiss-Penzias P. S., Coale K., Heim W., Fernandez D., Oliphant A., Dodge C., Hoskins D.,
855 Farlin J., Moranville R. and Olson A. (2016) Total- and monomethyl-mercury and major
856 ions in coastal California fog water: Results from two years of sampling on land and at sea.
857 *Elementa: Science of the Anthropocene*, 4: 000101, doi: 10.12952/journal.elementa.000101

858 **Figure Captions**

859 **Figure 1.** Study site in the Northwestern Mediterranean, with main circulation patterns.
860 Stations location during the CASCADE cruise (March 2011). Station coordinates are given in
861 Table S2.

862 **Figure 2.** Dissolved MeHg ($MeHgT_F$) *versus* salinity. (a) Estuarine mixing zone, (b) Low
863 Salinity Water lenses. The solid line represents the linear relationship between $MeHgT_F$ and
864 salinity ($MeHgT_F$ = - 0.0025*Sal + 0.1258, R^2 = 0.76), which suggests conservative mixing.

865 **Figure 3**. Time series of dissolved methylmercury ($MeHgT_F$) and salinity in the Low Salinity
866 Water lenses (LSWs) drifting on the Gulf of Lions' shelf and slope. Note that the LSW
867 lenses occur mainly in the top 0-20 m depth.

868 **Figure 4.** Methylmercury (MeHgT) vertical profiles in the water of the shelf (a) and the
869 continental slope (b) of the Gulf of Lions. UNF subscribes refer to unfiltered samples. Error
870 bars correspond to standard deviations of 2 to 4 samples collected during temporal
871 monitorings.

872 **Figure 5.** Vertical profiles of methylated mercury (MeHgT) in the North Gyre water column.
873 (a) Unfiltered ($MeHgT_{UNF}$) water samples and (b) MMHg/DMHg ratios.

874 **Figure 6**. (a) Isotopic composition of MeHgT after incubation (192 h) of slurries of surface
875 sediments in unfiltered bottom water and (b) gross methylation rates in incubations of
876 unfiltered seawater from the bottom of the shelf water column, showing increasing
877 methylation rates over time during the first 96h of incubation followed by the highest and
878 constant methylation rates after 96h. Error bars represent standard deviation for multiple
879 analyses (n=3) of the same sample. For the methylation rates, error bars estimated from
880 multiple injections of the same sample (n=3) were smaller than symbol size.

881 **Figure 7.** Relationships between methylated mercury (MeHgT) and dissolved oxygen (Dissolved O_2)
882 in unfiltered samples from the North Gyre stations. (a) Methylated mercury (MeHgT) and (b)
883 monomethylmercury (MMHg) and dimethylmercury (DMHg). The probability threshold ($p<0.01$) is
884 reached for $R^2 \geq 0.55$. No dissolved O_2 measurements were available for station "Antarès".

885

886

887 **Tables**

888 **Table 1.** Rhône River. A statistical summary of the concentrations in dissolved (X_F < 0.45µm)
889 and particulate (X_P > 0.45µm) HgT and MeHg, measured in the waters at Arles (Sta. SORA). HgT
890 values measured in 1994-1995 are from Cossa and Coquery (2005). SD: standard deviation; n:
891 number of samples.

	HgT_F (pmol L^{-1})	HgT_P (nmol g^{-1})	$MeHg_F$ (pmol L^{-1})	$MeHg_P$ (nmol g^{-1})
Average ± SD (n)	2.45 ± 2.05 (24)	0.85 ± 0.45 (27)	0.100 ± 0.035 (23)	0.017 ± 0.008 (26)
Min. – Max.	0.40 – 9.25	0.20 – 2.15	0.035 – 0.185	0.004 – 0.032

892

893

894

895 **Table 2.** Low Salinity Water lenses (LSW) and slope foot waters (SFW, Sta. S230). A statistical
896 summary of HgT and MeHgT (MeHgT=MMHg+DMHg) measurements during the BIOPRHOFI
897 cruise. Average ± standard deviation (number of samples) and range (Min. – Max.). (*) mean and
898 standard deviation were calculated with the 87 concentration values, which included 30
899 measurements lower than the detection limit, which have been put equal to the half of the
900 detection limit.

	HgT (pmol L^{-1})	MeHgT (pmol L^{-1})	MeHgT/HgT (%)
LSW (1-50 m layer; bottom ≤120 m) Filtered samples (<0.4µm)	1.57 ± 0.74 (84) 0.61 – 3.50	0.021*± 0.012* (87) <0.015 – 0.069	1.5 ± 1.0 (84) <0.3 – 5.5
SFW (< 100 m layer; bottom at 1386 m) Unfiltered samples	1.22 ± 0.13 (3) 0.98 – 1.35	0.13 ± 0.10 (7) 0.026 – 0.241	10 ± 7 (3) 2 – 18
SFW (100-900 m layer; bottom at 1386 m) Unfiltered samples	1.41 ± 0.06 (4) 1.33 – 1.48	0.32 ± 0.13 (11) 0.23 – 0.38	18 ± 1 (4) 16 – 20

901

902

903

904 T**able 3.** Gulf of Lions shelf, slope and North Gyre waters (CASCADE cruise). Summary
905 statistics for HgT_{UNF} and $MeHgT_{UNF}$ concentrations. Average ± Standard deviation (number of
906 samples) and range (Min. – Max.). Station locations are indicated on figure 1 and coordinates
907 are given on table S2. (*) Values calculated with concentrations lower than the DL put equal to
908 the half of the DL.

Station (water layer sampled)	HgT_{UNF} (pmol L^{-1})	$MeHgT_{UNF}$ (pmol L^{-1})	$MeHgT_{UNF}/HgT_{UNF}$ (%)
Inner shelf (bottom <100 m)			
A (1-90 m)	2.04 ± 1.11 (7)	0.041 ± 0.034 (9)*	1.5 ± 0.9 (7)
	1.27 – 4.47	<0.015 – 0.119	0.6 – 3.4
B (1-90 m)	1.17 ± 0.29 (10)	0.034 ± 0.021 (10)*	3.1 ± 2.2 (10)
	0.78 – 1.61	<0.015 – 0.066	0.5 – 6.3
C (1-90 m)	1.40 ± 1.08 (10)	0.007 ± 0.009 (11)*	0.9 ± 1.8 (10)
	0.58 – 4.20	<0.015 – 0.035	0.1 – 6.0
D (1-90 m)	1.61 ± 1.23 (9)	0.024 ± 0.014 (10)*	2.2 ± 1.7 (9)
	0.92 – 3.80	<0.015 – 0.048	0.3 – 5.1
A/B/C/D (1-90m)	1.52 ± 1.00 (36)	0.026 ± 0.024 (40)*	1.9 ± 1.9 (36)
	0.58 – 4.47	<0.015 – 0.119	0.1 – 6.3
Slope edge and head of the Cap de Creus canyon (bottom at 100-300 m)			
E (2-290 m)	0.99 ± 0.52 (20)	0.026 ± 0.048 (8)*	1.5 ± 2.0 (8)
	0.58 – 2.94	<0.015 – 0.141	0.3 – 4.7
L-01 (5-250 m)	1.07 ± 0.10 (6)	0.033 ± 0.023 (6)	3.0 ± 1.8 (6)
	1.00 - 1.26	0.020 – 0.076	1.8 – 6.1
M-12 (10-130 m)	1.02 ± 0.12 (4)	0.049 ± 0.006 (4)	4.8 ± 0.8 (4)
	0.93 – 1.14	0.042 – 0.056	4.1 – 6.0
Slope foot (bottom at 900-1800 m)			
M-10 (10-1100 m)	1.01 ± 0.15 (10)	0.271 ± 0.088 (10)	26.2 ± 6.2 (10)
	0.66 – 1.13	0.092 – 0.355	13.9 – 33.4
L-03 (10-1860 m)	1.22 ± 0.12 (10)	0.177 ± 0.077 (8)	14.9 ± 6.5 (8)
	1.13 – 1.53	0.020 – 0.266	1.3 – 22.0

North Gyre (bottom at > 2000 m)			
Antarès (10-2500m)	1.05 ± 0.12 (9)	0.235 ± 0.107 (9)	21.8 ± 8.8 (9)
	0.84 – 1.23	0.090 – 0.375	11.3 – 33.8
L-05 (10-2200 m)	1.04 ± 0.04 (10)	0.252 ± 0.040 (9)	24.3 ± 3.9 (9)
	0.98 – 1.11	0.199 – 0.309	18.8 – 30.1
L-08 (10-2150 m)	1.07 ± 0.04 (10)	0.307 ± 0.045 (10)	28.7 ± 4.3 (10)
	1.01 – 1.13	0.263 – 0.394	24.2 – 38.6
L-10 (10-2360 m)	1.02 ± 0.12 (10)	0.314 ± 0.113 (10)	30.2 ± 8.4 (10)
	0.82 – 1.11	0.166 – 0.478	20.3 – 43.2
L-12 (10-2500m)	1.13 ± 0.18 (10)	0.237 ± 0.079 (10)	21.3 ± 5.1
	0.64 – 1.23	0.136 – 0.398	13.4 – 32.4
S2400 (10-2400m)	1.11 ± 0.01 (10)	0.175 ± 0.123 (10)	15.8 ± 11.1 (10)
	1.08 – 1.12	0.020 – 0.326	1.8 – 25.4
M-08 (10-2010m)	1.15 ± 0.12 (10)	0.305 ± 0.052 (10)	26.8 ± 5.9 (10)
	1.03 – 1.45	0.245 – 0.367	17.7 – 35.7
M-05 (10-2490 m)	1.14 ± 0.04 (10)	0.216 ± 0.062 (10)	18.8 ± 5.5 (10)
	1.05 – 1.19	0.106 – 0.302	10.0 – 26.9
M-03 (10-2580 m)	1.24 ± 0.10 (10)	0.276 ± 0.056 (10)	22.6 ± 5.5 (10)
	1.09 – 1.41	0.137 – 0.320	9.7 – 27.9
M-01 (10-2500 m)	1.06 ± 0.24 (10)	0.278 ± 0.132 (10)	24.7 ± 8.7 (10)
	0.53 – 1.24	0.066 – 0.374	8.9 – 34.6

921 T**able 4.** Gulf of Lions shelf and North Gyre (CASCADE cruise). Summary statistics for $MeHgT_F$
922 (<0.4μm) in the first 2 cm of the sediment pore waters and bottom water (10 cm above the water sediment
923 interface). The thickness of the oxidized layer (cm) is based on the redox potential value. In italic and
924 brackets are the MeHgT concentrations (pmol g^{-1}) in the solid phase.
925

Station	Oxidized layer thickness (cm)	$MeHgT_F$ (pmol L^{-1}) Pore water	$MeHgT_F$ (pmol L^{-1}) Bottom water
Inner shelf (bottom <100 m)			
A-04	2	0.071 *(4.0)*	0.022
B-05	3	0.268 *(3.5)*	0.008
C-05	3	0.684 *(3.0)*	0.040
D-06	4.5	0.254 *(3.5)*	0.040
E-03	-	0.259	0.040
E-08	4.5	0.258	0.040

926
927

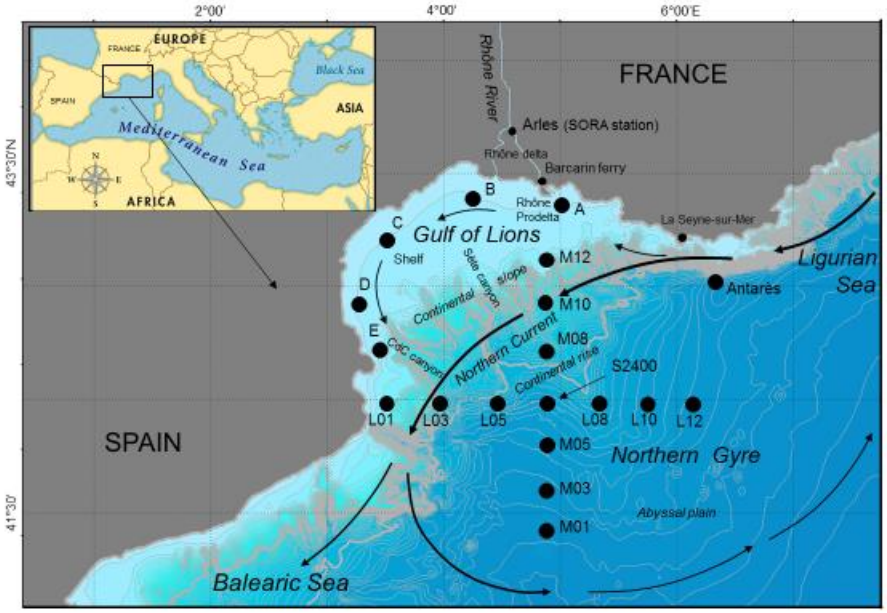

Fig. 1

928
929

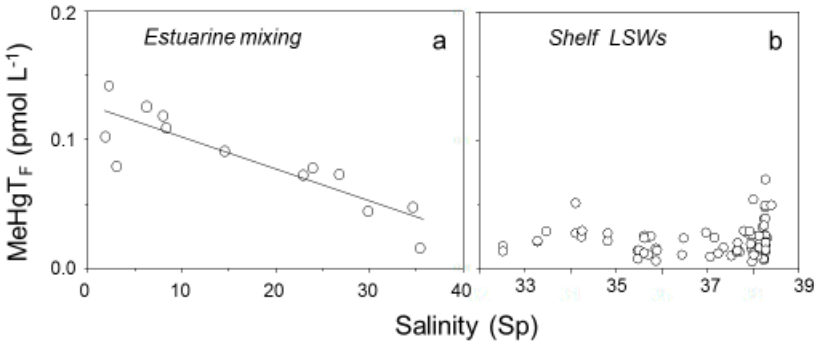

Fig. 2

930
931
932
933
934
935

936

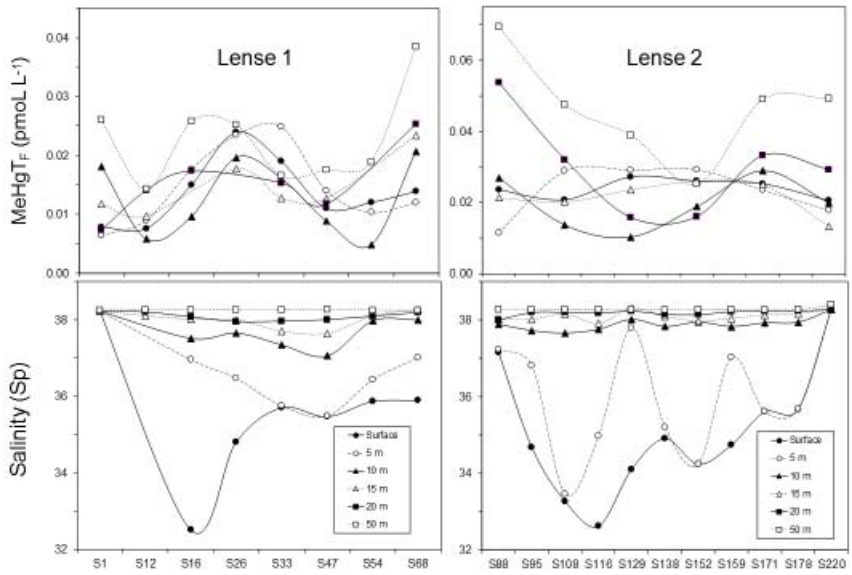

Fig. 3

937
938

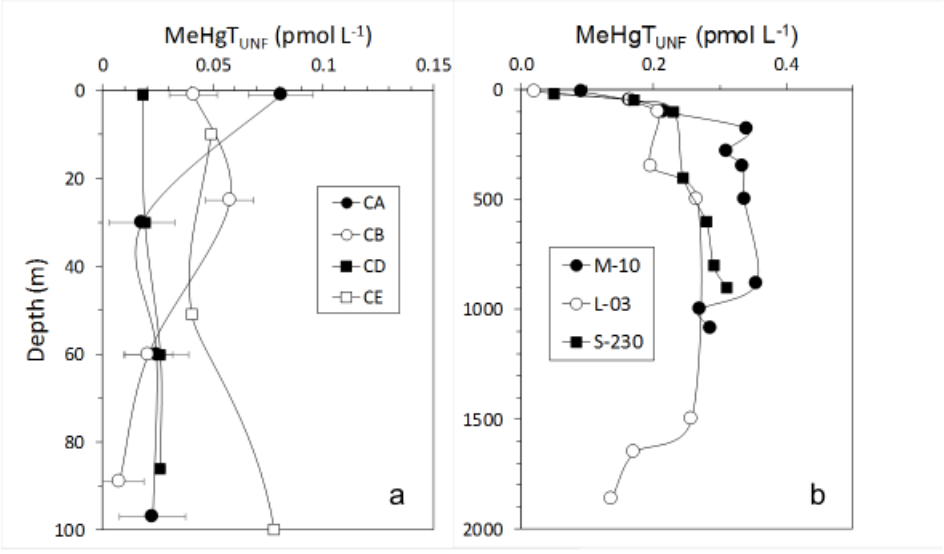

Fig. 4

939
940
941
942
943
944

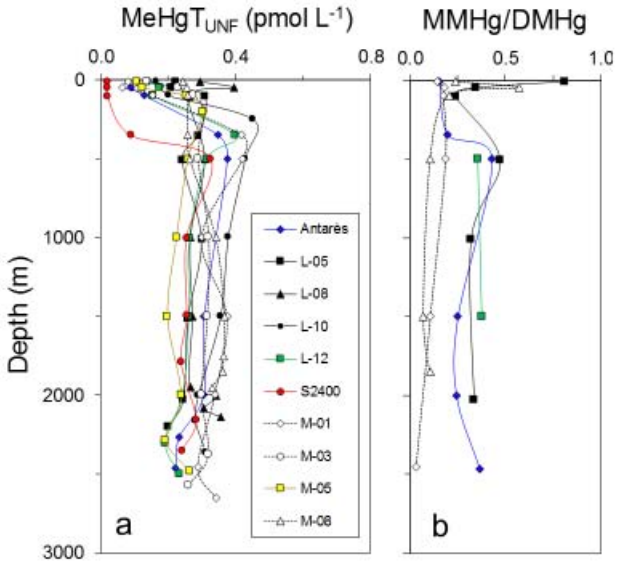
MeHgT$_{UNF}$ (pmol L^{-1})
MMHg/DMHg
0.0
0.4
0.8
0.0
0.5
1.0
0
1000
2000
3000
Depth (m)
Antarès
L-05
L-08
L-10
L-12
S2400
M-01
M-03
M-05
M-06
a
b

Fig. 5

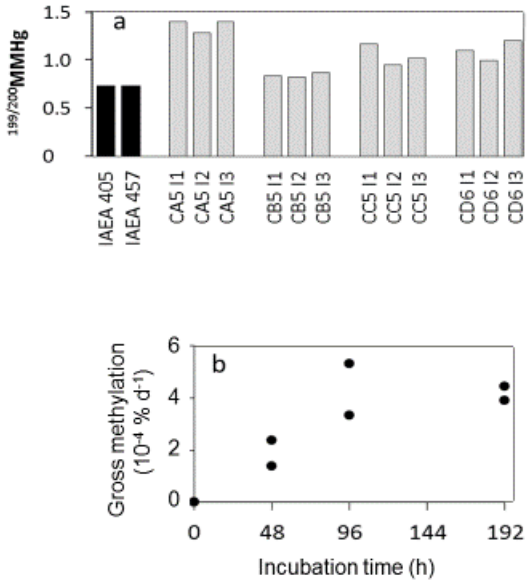
a
$^{199/200}$MMHg
1.5
1.0
0.5
0
IAEA 405
IAEA 457
CA5 I1
CA5 I2
CA5 I3
CB5 I1
CB5 I2
CB5 I3
CC5 I1
CC5 I2
CC5 I3
CD6 I1
CD6 I2
CD6 I3
b
Gross methylation
(10^{-4} % d^{-1})
6
4
2
0
0
48
96
144
192
Incubation time (h)

Fig. 6

954

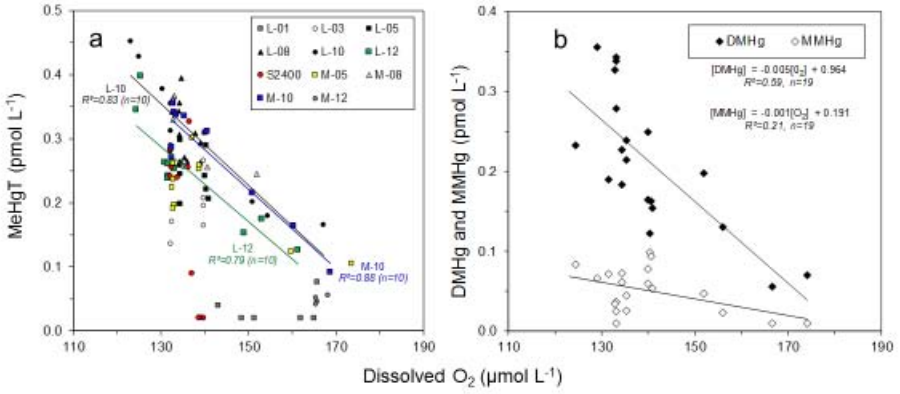

Fig. 7

955
956

957 **Supplementary material including Suppl. Figures (S1-S6), Suppl. Tables (S1 and S2),**
958 **Suppl. Information (SI1, SI2 and SI3) and references**

959

960 **Supplementary Figure Captions**

961 **Figure S1**. Schematic representation of the Gulf of Lions water circulation patterns.

962 **Figure S2.** Trajectories of the desalted water lenses (LSWs) drifting on the Gulf of Lions' shelf and
963 slope.

964 **Figure S3**. Potential temperature vertical profiles along the "L" transect (Fig. 1). Stratified stations are
965 characterized by high temperature gradients (red zones), whereas homogenized water column are
966 illustrated by a bleu monocolor.

967 **Figure S4**. Particulate methylmercury ($MeHg_P$) *versus* (a) particulate phosphorus, and (b) pigments at
968 stations 221 and 230. See figure S2 for station locations.

969 **Figure S5**. Dissolved methylmercury versus particulate methylmercury in desalted water lenses (LSW)
970 drifting on the Gulf of Lions' shelf and slope. See figure S2 for station locations.

971 **Figure S6.** Dissolved methylmercury ($MeHg_F$) *versus* dissolved oxygen within desalted water lenses
972 (LSW) drifting on the Gulf of Lions' shelf and slope. See figure S2 for station locations.

973

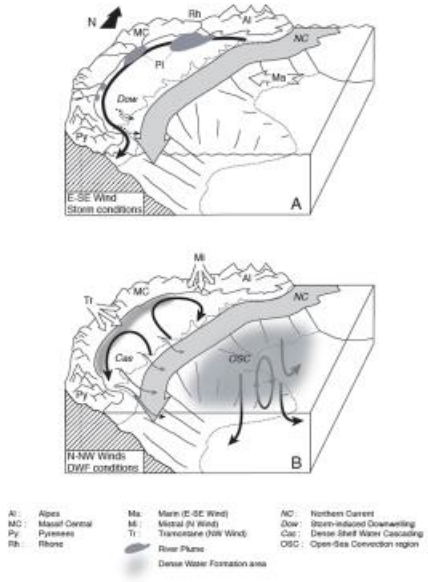

Fig. S1

974

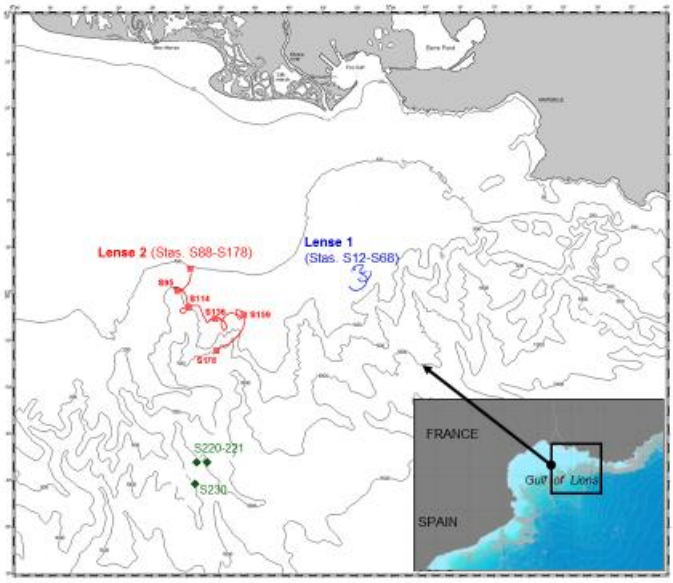

Fig. S2

975

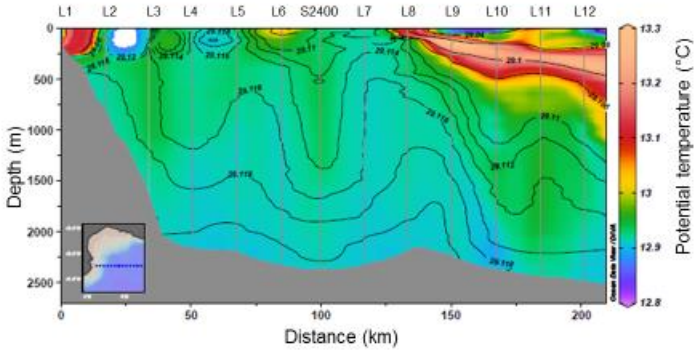

Fig. S3

976

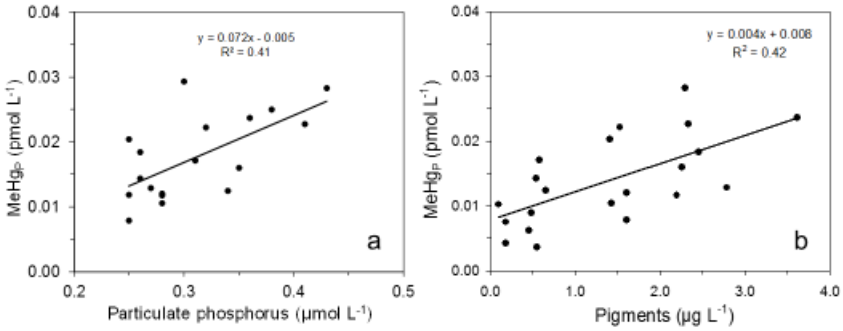

Fig. S4

977

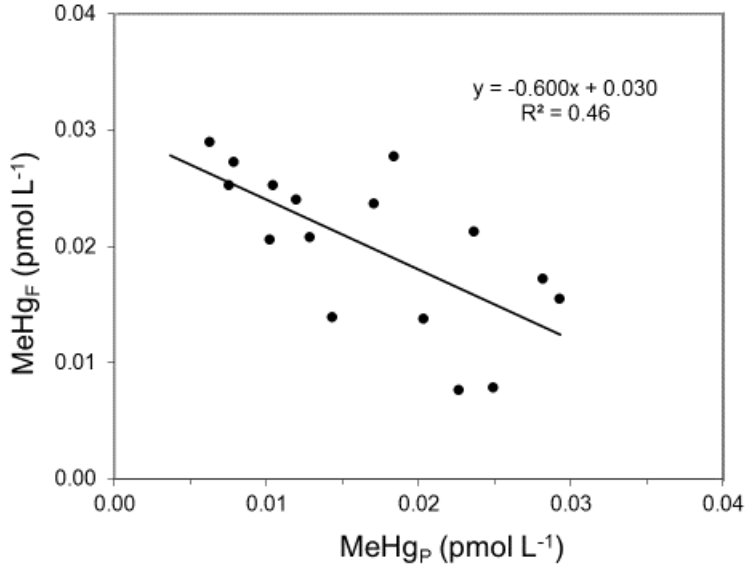

Fig. S5

978

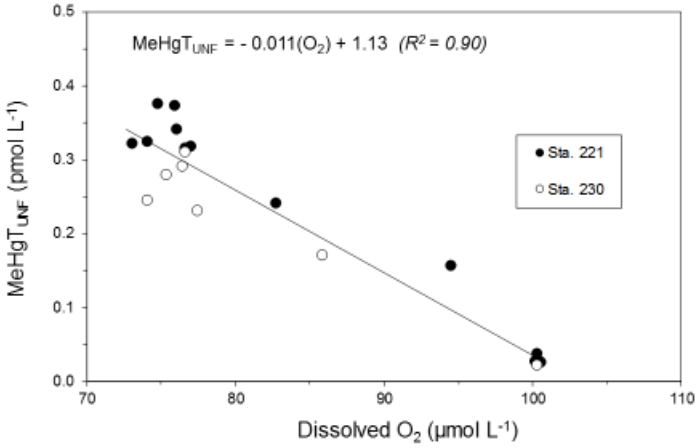

Fig. S6

979

980

Supplementary Tables

Table S1. Sampling cruises. (1) http://www.com.univ-mrs.fr/MOOSE/spip.php?article46; (2) http://www.smtdr.fr/page5.html; (3) http://flotte.ifremer.fr/fleet/Presentation-of-the-fleet/Vessels/Deep-sea-vessels/Le-Suroit/Virtual-tour-of-N-O-Le-Suroit; (4) http://flotte.ifremer.fr/fleet/Presentation-of-the-fleet/Vessels/Deep-sea-vessels/L-Atalante. See also the map on figure 1.

Name of the cruise	Location of the sampling	Mode of collection	Date	Type of samples collected
Rhône monitoring project	Rhône River at Arles	SORA pumping station[1]	April to June and October to November 2008	Particles
			March 2009 to June 2010	Filtered waters and particles
Rhône delta study	Rhône fresh-seawater mixing zone	Barcarin ferry[2] and Zodiac	October 2008	Filtered waters and particles
BIOPRHOFI cruise	Shelf and slope	R/V Suroit[3]	May 2006	Filtered and unfiltered waters. and particles
CASCADE cruise	Shelf, slope, canyon and rise	R/V Atalante[4]	March 2011	Filtered and unfiltered waters and sediment cores (solid and pore waters)
Atmospheric monitoring	Coastal site (La Seyne-sur-Mer)	Rain collector	April 2009 to January 2010	Wet and dry deposition

994
995
996 **Table S2a**. Water sampling stations: Cruise, coordinates and bottom depth.
997

Cruise	Station	Latitude (N)	Longitude (E)	Bottom depth (m)
Rhône River monitoring	SORA (Arles)	43°40.722’	4°.37.278’	4
Rhône mixing zone	I-II	43°.15.360’	4°26.460’	6
Rhône mixing zone	III-IV	43°15.012’	4°26.892’	8
Rhône mixing zone	V-VII	43°15.018’	4°26.862’	13
Rhône mixing zone	VIII-XIV	43°13.758’	4°28.968’	10
BIOPRHOFI	S12	43°05.555’	4°47.848’	104
BIOPRHOFI	S16/18	43°02.395’	4°54.328’	123
BIOPRHOFI	S26	43°03.156’	4°55.379’	120
BIOPRHOFI	S33	43°02.857’	4°56.328’	123
BIOPRHOFI	S47	43°02.066’	4°57.294’	123
BIOPRHOFI	S54	43°02.008’	4°55.098’	123
BIOPRHOFI	S68	43°00.897’	4°54.132’	122
BIOPRHOFI	S88	43°03.014’	4°30.747’	103
BIOPRHOFI	S95	43°00.035’	4°28.624’	267
BIOPRHOFI	S108	42°58.267’	4°29.126’	358
BIOPRHOFI	S116	42°58.095’	4°31.054’	132
BIOPRHOFI	S129	42°56.984’	4°32.381’	131
BIOPRHOFI	S138	42°56.986’	4°34.895’	131
BIOPRHOFI	S152	42°57.621’	4°36.471’	127
BIOPRHOFI	S159	42°57.746’	4°38.387’	125
BIOPRHOFI	S171	42°55.144’	4°37.313’	269
BIOPRHOFI	S178	42°53.911’	4°34.218’	495
BIOPRHOFI	S220	42°42.374’	4°36.422’	971
BIOPRHOFI	S221	42°41.884	4°32.451’	1122
BIOPRHOFI	S230	42°34.071’	4°27.957’	1386
CASCADE	Antarès	42°48.150’	6°07.466’	2497
CASCADE	L01	42°01.950’	3°29.284’	239
CASCADE	L03	42°01.967’	3°53.250’	1887
CASCADE	L05	42°01.998’	4°17.400’	2199
CASCADE	L08	42°02.017’	5°06.067’	2166

CASCADE	L10	42°01.998’	5°30.150’	2398
CASCADE	L12	42°55.9845	5°41.816’	2536
CASCADE	S2400	42°02.000’	4°41.533’	2391
CASCADE	M01	41°08.033’	4°41.750’	2691
CASCADE	M03	41°25.967’	4°41.783’	2614
CASCADE	M05	41°44.033’	4°41.466’	2522
CASCADE	M08	41°19.984’	4°41.816’	1979
CASCADE	M10	42°19.988’	4°41.850’	1096
CASCADE	M12	42°55.984’	4°41.816’	126
CASCADE	A-08	43°12.984’	04°50.371’	99
CASCADE	B-08	43°12.570’	04°07.670’	91
CASCADE	C-08	42°56.054’	03°29.580’	93
CASCADE	D-09	42°38.515’	03°18.408’	90
CASCADE	E-06	42°20.725’	03°21.414’	280
CASCADE	X-1 to X-33	42°20.867’	3°21.484’	290

998

999

1000 **Table S2b**. Sediment sampling stations: Cruise, coordinates and bottom depth.
1001

Cruise	Station	Latitude (N)	Longitude (E)	Bottom depth (m)
CASCADE	A-04	43°18.092’	04°50.635’	57
CASCADE	B-05	43°20.375’	04°08.127’	64
CASCADE	C-05	43°03.382’	03°22.305’	60
CASCADE	D-06	42°40.594’	03°10.800’	61
CASCADE	E-03	42°19.951’	03°20.943’	120
CASCADE	E-08	42°21.106’	03°22.029’	442
CASCADE	S2400	42°01.985’	04°41.807’	2333
CASCADE	M01	41°08.005’	04°41.798’	2625
CASCADE	M08	42°19.989’	04°41.832’	1942

1002

1003

Supplementary Information

SI1. Methods

Sample treatment

Water and particles. The samples from the 0-50 m layer of the shelf waters during the BIOPRHOFI cruise were collected by pumping with an all-Teflon pneumatic pump (10-2PM, ASTI®) and through polyethylene tubing, directly into a class 100 on-board container, with the consequence that the seawater was never in contact with the atmosphere of the ship. All the plastic wares were previously acid-cleaned according to ultraclean sample handling protocols (e.g., Cossa et al. 2003). Discrete water samples were collected in 2L Teflon (FEP) bottles inside the container, where filtrations were then performed on sub-samples using acid washed polycarbonate membranes (0.45 µm, Nuclepore®). Filtrate (250 mL) was collected in Teflon (FEP) bottles and acidified with HCl (0.4 %, v/v, Suprapur, Merck®) for subsequent analyses of "dissolved" fraction of total and methylmercury (HgT_F and $MeHgT_F$). The collection of particles from the Low Salinity Waters, for subsequent $MMHg_P$, CHNP and pigments determinations, was performed using in-line filtration through glass fiber filters (GF/G, Whatman®) previously cleaned by heating at 450°C for 24h and mounted in a Teflon (PTFE)/stainless steel filter holder (∅142 mm, Schleicher & Schuell®) within the container. Up to 60 liters of water were filtered this way in order to collect enough material for the various particulate analyses. Samples for dissolved gaseous Hg (DGM) analyses were collected in a 1L Teflon bottle (FEP) according to the traditional method used for dissolved oxygen determination in order to avoid gas evasion during the collection. Deep-water samples (> 50 m) were collected during the BIOPRHOFI and CASCADE cruises by rosette-mounted 5L bottles (1010X-Niskin, General Oceanics®) equipped with a CTD probe. These samples were not filtered and analyzed only for HgT_{UNF} and $MeHgT_{UNF}$. Dissolved gaseous Hg and HgT were determined on board, while MMHg and MeHgT analyses were performed in the laboratory within 2 months after the cruise on the acidified samples stored in the dark at +4°C in a double wrapping of polyethylene bags.

Sediment cores: The cores were collected along the Gulf of Lions shelf, at the head of the Cap de Creus canyon and in the abyssal plain in the North Gyre area during the CASCADE cruise. A multicore sampler (Oktopus GmbH Multiple corer with 8 tubes of 100 mm diameter) allowing the sampling of the undisturbed benthic interface (Barnett et al., 1984) was used. The pore water was drained using Milli-Q (Millipore®) water-rinsed microporous polymer tube samplers (Rhizon SMS, Rhizosphere Research Products®) fixed on an acid washed all-polypropylene syringe (Guédron et al., 2012). Collected pore water (the two first cm below the water-sediment interface) was filtered through a

hydrophilic Teflon membrane (0.45 µm, Millex-LCR, Millipore®), then acidified with high purity HCl (0.4 % v/v, Suprapur, Merck®) and stored in the dark until MMHg analysis. According to Guédron et al. (2012), Rhizon samplers preferentially recover water from the sediment macropores, containing the readily exchangeable chemical species.

Chemical analyses

Total mercury. Total Hg in filtered and unfiltered samples were measured on board within a few minutes of sampling. In order to access all the mercury chemical species, present in the sample, the release of Hg from its ligands was achieved by a BrCl solution (0.1 mL of a 0.2 M solution is added to a 100 mL sample), and then the Hg^{II}_i was reduced to Hg^0 with an acidic $SnCl_2$ solution (0.2 mL of a 1 M solution is added to a 100 mL sample). This technique derives from the original Bloom and Crecelius (1983) method and has been described in detail by several authors (e.g., Gill and Fitzgerald, 1988; Horvat et al., 1991; Mason and Fitzgerald, 1993) and is now known as the US-EPA standard method N° 1631. The Hg^0 vapor generated by the reduction is amalgamated on a gold (Au) trap then released by heating into an Atomic Fluorescence Spectrometer (2500, Tekran®). For both measurements, the detection limit (DL) was 0.1 pmol L^{-1} and the reproducibility varied according to the concentration level between 5 and 15 % (Cossa et al. 2003). The accuracy of HgT measurements was tested using the ORMS-3 certified reference material (CRM) from the National Research Council of Canada. Our measurements were always within the confidence limits given for the CRM (12.6 ± 1.1 pg mL^{-1}; http://inms-ienm.nrc-cnrc.gc.ca/calserv/crm_files_f/ORMS-3_f.pdf).

Methylated Hg species. Total methylated Hg and MMHg were measured on filtered and unfiltered samples, whereas DMHg was not measured, but calculated as the difference between $MeHgT_{UNF}$ and $MMHg_{UNF}$. Total methylated Hg was determined on acidified samples, which means that both MMHg and DMHg were determined in the same time, since DMHg is converted into MMHg at low pH (Mason, 1991; Black et al., 2009a). Monomethyl Hg was determined with the same technique as MeHgT, but after bubbling 350 mL samples for 40 min with argon (Ar) at a flow rate of 250 mL min^{-1} in order to remove DMHg before acidification. Total methylated Hg and MMHg were determined as volatile MMHg hydride by purge and cryo-trapping gas chromatography and detected as elemental Hg vapor by atomic fluorescence spectrometry (AFS). The mercury hydrides (from MMHg and Hg^{II}_i) were formed with $NaBH_4$, sparged from the sample with helium (He) (250 mL min^{-1}), concentrated and then separated (50 mL min^{-1}) by cryogenic chromatography before being converted in Hg^0 in a furnace (800°C) and detected by the AFS detector. The hydride generation technique was initially proposed by Filippelli et al. (1992), modified by Tseng et al. (1998), and then improved by Stoichev et al. (2004) and Cossa et al. (2009). Last authors optimized the method in order to detect sub-picomolar

1069 levels in seawater by lowering the reagent amount (addition of only 0.6-4.0 mL of a $NaBH_4$ solution of
1070 0.5 % (w/v) to a 30-200 mL water sample) and using a very stable and sensitive detector with an
1071 absolute DL of ~1 femtomol of Hg (AFS detector 2500 model equipped with a mirror-coated quartz
1072 cuvette, Tekran®). The hydrides are formed within a silanized borosilicate glass reactor (5 % DMDCS
1073 in toluene), then concentrated at low temperature (in liquid nitrogen) and separated by heating (up to
1074 90°C) in a silanized borosilicate glass tube of 4 mm interior diameter and filled with Chromosorb
1075 WAW-DMCS (60/80 mesh impregnated with 15 % OV-3). The vector gas was Hg-free He, purified
1076 by passing through charcoal and gold filters. During this set of analyses, the blank (< 0.01 pmol) and
1077 its reproducibility (2 %) allowed DLs (calculated as 3 times the standard deviation of the blank)
1078 ranging from 0.005 to 0.025 pmol L^{-1} depending on the volume of the sample analyzed, and limits of
1079 quantification (calculated as 10 times the standard deviation of the blank) ranging from 0.015 to 0.075
1080 pmol L^{-1}. The analytical reproducibility varied with time between 6 and 15 %. The accuracy was not
1081 directly estimated because no certified reference seawater for MMHg was available. The calibration
1082 was performed using the dilutions of a 1 g L^{-1} stock MMHg solution in isopropanol. The dilutions of
1083 the stock solution were performed in HCl (0.4 %, w/v, Suprapur, Merck®) water solution. Three times
1084 a day, 2 µL of saturated Hg^0 vapor was injected into the chromatographic system through a septum in
1085 order to check the response of the instrument and verify the hydride yields. Details of the analytical
1086 system are given in a technical paper (Cossa et al. 2003).

1087 $MeHgT_P$ was determined by atomic fluorescence spectrometry after HNO_3 (4M, Suprapur,
1088 Merck®) extraction, ethylation of the MMHg and Hg^{II}_i, followed by chromatographic separation of the
1089 volatile ethylated compounds according to Liang et al. (1994). The accuracy, reproducibility and DL,
1090 established analyzing a Certified Reference Material from the International Atomic Energy Agency
1091 (IAEA-142, Horvat et al., 1997), were 80-120 % (recovery), 10 % (coefficient of variation) and 4 ng g^{-1}
1092 (3 times the standard deviation of the blank).

1093 *Dissolved gaseous Hg*. For analysis of DGM, 300 mL of sample was purged for 30 min with ultra-high
1094 purity nitrogen stripped of Hg^0 by passage through Au traps, at a flow rate of 300 L min^{-1},
1095 corresponding to a calculated extraction rate of 78 % (results were corrected for this yield). Volatilized
1096 Hg species were trapped and concentrated on an Au trap (Braman and Johnson, 1974), subsequently
1097 desorbed by pyrolysis and quantified by gas-phase AFS. Dissolved gaseous Hg net production was
1098 evaluated by incubating unfiltered water samples in an incubator located on the deck of the vessel
1099 exposed to sunlight radiations. Temperature was controlled by continuously pumping sea-surface
1100 water through the incubator using a through-flow system. These *ex-situ* incubations were performed in
1101 batch experiments during 2 to 12 h periods under the following conditions: (i) absence of light (FEP

Teflon bottles, wrapped in Al foil); (ii) presence of light (FEP Teflon bottles). Transparent FEP Teflon bottles absorbed 2.5 % of total incident radiation according to Amyot et al. (1997). Net DGM production was estimated without taking into account the possible re-oxidation of Hg^0.

SI2. Riverine flux calculations

In the absence of any significant relationship between "dissolved" HgT and RR water discharge the HgT_F flux was calculated as the product of weighted average of Hg concentrations and average discharge (Meybeck and Ragu, 1996; Gairoard et al. 2012). On the contrary, in the case of particulate Hg, we took into account the existing HgT_P dependencies upon hydrological changes (Fig. 3). Rhône river discharge and the suspended particulate matter concentrations were obtained from the Compagnie Nationale du Rhône (http://www.cnr.tm.fr/). In these conditions, the HgT discharging from the RR between June 2009 and June 2010 has been calculated to be 85 and 800 mol as "dissolved" and particulate, respectively.

Considering that during the studied period the Rhône discharge was atypically low, and using the water and particulate mean discharges calculated on the basis of the last 36 years (Gairoard et al., 2012) the annual HgT efflux from the Rhône River to the GoL would be close to 2.7 and 0.13 kmol for the particulate and "dissolved" phases respectively. Assuming average ratios of MeHg/HgT of 1.9 and 4.1 % (Table 1 of the main manuscript), the best estimates of the MeHg annual Rhône effluxes is calculated to be 51 and 5 mol for particulate and the "dissolved" phases, respectively.

SI3. Modeling the diffusive fluxes

$MeHg_F$ diffusive fluxes were estimated at the stations A to E benthic boundary layer (BBL) using Fick's first law (Eq. 1):

$$J = - (\varphi D_w / \theta^2) (\delta C / \delta x)_{BBL} \quad [1]$$

Where, J is the flux of the solute with concentration C at depth x, φ is the sediment porosity (Eq. 2), θ is the tortuosity (Eq. 3), and D_w is the molecular diffusion coefficient of the solute in seawater. Measuring porosity, the tortuosity was approached using Boudreau's formulation:

$$\varphi = \text{pore water volume} / (\text{solid volume} + \text{pore water volume}) \quad [2]$$

$$\theta^2 = 1 - \ln(\varphi^2) \quad [3]$$

1130 The *Dw* for $MeHg_F$ as MeHgCl were determined coupling the linear regressions of the infinite
1131 dilution diffusion for cations and anions against temperature (Boudreau, 1996) with the infinite-dilution
1132 diffusion for ion pairs (Applin and Lasaga, 1984). The expression was calculated for temperature salinity
1133 and pressure from an empirical equation developed by Kukulka et al. (1987). The adjustment for pore
1134 water viscosity of normal seawater was small at no more than 7 % (Li and Gregory, 1974). The respective
1135 approximations for $MeHg_F$ at T = 18 °C, S = 35 and P = 2 bar were 1.84×10^{-5} and 8.65×10^{-6} $cm^2\ s^{-1}$.
1136
1137 **Table**: $MeHgT_F$ diffusive fluxes from shelf sediments in the Gulf of Lions (Northwestern Mediterranean).
1138 The MeHg gradient at the sediment-water interface is estimated using the difference between MeHg
1139 concentrations in surface sediment pore waters (2 cm below the interface) and bottom waters (10 cm
1140 above the water sediment interface).

Station	$MeHgT_F$ (pmol m^2 day^{-1})	$MeHgT_F$ (pmol L^{-1})
	Flux	$Diff_{Pore\ water\ and\ Bottom\ water}$
A-04	0.20	0.049
B-05	1.04	0.26
C-05	2.58	0.644
D-06	0.86	0.214
E-03	0.88	0.219
E-08	0.87	0.218

1141
1142

1143 **References for SI1-3**

1144 Applin, K.R. and A.C. Lasaga. 1984. The determination of $SO4^{2-}$, $NaSO4^-$, and MgSO4 tracer diffusion
1145 coefficients and their application to diagenetic flux calculations. *Geochim. Cosmochim. Acta,* 48:
1146 2151–2162.

1147 Barnett P.R.O., Watson J. and Connelly D. (1984) A multiple corer for taking virtually undisturbed
1148 samples from shelf, bathyal and abyssal sediments. *Oceanol. Acta*, **7**, 399-408.

1149 Black F. J., Conaway C. H. and Flegal A. R. (2009) Stability of Dimethyl Mercury in Seawater and
1150 Its Conversion to Monomethyl Mercury. *Environ. Sci. Technol*., **43**, 4056-4062.

1151 Bloom N. S. and Crecelius E. A. (1983) Determination of mercury in seawater at sub-nanogram per
1152 liter levels. *Mar. Chem*., **14**, 49-59.

1153 Boudreau, B.P. 1996. Diffusive tortuosity on fine-grained unlithified sediments. *Geochim. Cosmochim.*
1154 *Acta*, 60: 3139-3142.

1155 Braman R. S. and Johnson D. L. (1974) Selective Absorption Tubes and Emission Technique for
1156 Determination of Ambient Forms of Mercury in Air. *Environ Sci. Technol*., **8**, 996-1003.

1157 Cossa D., Averty B., Breaudeau J. and Senard A.-S. (2003) *Spéciation du mercure dissous dans les*
1158 *eaux marines. Analytical methods for the marine environments*. Ifremer and French Ministry for
1159 Ecology and Sustainable Development publication MA0303.

1160 Cossa D., Averty B. and Pirrone N. (2009) The origin of methylmercury in open Mediterranean
1161 waters. *Limnol. Oceanogr.,* **54**, 837-844.

1162 Filippelli M., Baldi F., Brinckman F. E. and Olson G. J. (1992) Methylmercury Determination as
1163 Volatlle Methylmercury Hydride by Purge and Trap Gas Chromatography in Line with Fourier
1164 Transform Infrared Spectroscopy. *Environ. Sci. Technol*., **26**, 1457-1460.

1165 Gairoard, S., O. Radakovitch, F. Eyrolle, W. Ludwig and D. Cossa. 2012. *Flux de matière solides et*
1166 *liquides des bassins versants français à la Méditerranée*. Rapport IRSN, CEREGE, UPVD, IFREMER à
1167 l'AERMC, Septembre 2012. 87 pages.

1168 Gill G. A. and Fitzgerald W. F. (1988) Vertical mercury distribution in the oceans. *Geochim*.
1169 *Cosmochim. Acta*, **52**, 1719-1728.

1170 Guédron S., Huguet L., Vignati D. A. L., Liu B., Gimbert F., Ferrarin B. J. D., Zonta R.and Dominik J.
1171 (2012) Tidal cycling of mercury and methylmercury between sediments and water column in the
1172 Venice Lagoon (Italy). *Mar. Chem*., **130-131**, 1-11.

1173 Horvat M., Lupsina V. and Pihlar B. (1991) Determination of total mercury in coal fly ash by gold
1174 amalgamation cold vapour atomic absorption spectrometry. *Anal. Chim. Acta,* **243**, 71-79.

1175 Kukulka, D.J., B. Gebhart and J.C. Mollendorf. 1987. Thermodynamic and transport properties of pure
1176 and saline water. *Advanced Heat Transfer,* 18: 325-363.

1177 Li, Y.-H. and S. Gregory. 1974. Diffusion of ions in seawater and in deep-sea sediments. *Geochim.*
1178 *Cosmochim. Acta*, 38: 703-714.

1179 Liang L., Horvat M. and Bloom N. S. (1994) An improved speciation method for mercury by
1180 GC/CVAFS after aqueous phase ethylation and room temperature precollection. *Talanta*, **41**, 371-
1181 379.

1182 Mason R. P. (1991) *The chemistry of mercury in the equatorial Pacific Ocean*. PhD Thesis. University
1183 of Connecticut, USA, 305 pp.

1184 Mason R. P. and Fitzgerald W. F. (1993) The distribution and biogeochemistry cycling of mercury in
1185 the Equatorial Pacific Ocean. *Deep-Sea Res. I*, **40**, 1897-1924.

1186 Meybeck, M. and A. Ragu. 1996. *River discharges to the oceans: an assessment of suspended solids,*
1187 *major ions and nutrients*. Division Environment, Information and Assessment (Water Branch) Report,
1188 UNEP, Nairobi, 256 pp.

1189 Stoichev T. R., Rodriguez Martin-Doimeadios C., Tessier E., Amouroux D. and Donard O. F. X.
1190 (2004) Improvement of analytical performances for mercury speciation by on-line derivatization,
1191 cryofocussing and atomic fluorescence spectrometry. *Talanta,* **62**, 433-438.

1192 Tseng C. M., de Diego A., Pinaly H., Amouroux D. and Donard O. F. X. (1998) Cryofocusing
1193 coupled to atomic absorption spectrometry for rapid and simple mercury speciation in
1194 environmental matrices. *J. Anal. At. Spectrom*., **13**, 755-764.
1195